ASSESSMENT OF TSUNAMI RESILIENCE OF PORTS BY HIGH RESOLUTION NUMERICAL MODELING: A CASE STUDY FOR HAYDARPASA PORT IN THE SEA OF MARMARA

A THESIS SUBMITTED TO
THE GRADUATE SCHOOL OF NATURAL AND APPLIED SCIENCES
OF
MIDDLE EAST TECHNICAL UNIVERSITY

BY

BETÜL AYTÖRE

IN PARTIAL FULFILLMENT OF THE REQUIREMENTS
FOR
THE DEGREE OF MASTER OF SCIENCE
IN
CIVIL ENGINEERING

JANUARY 2015

Approval of the thesis:

ASSESSMENT OF TSUNAMI RESILIENCE OF PORTS BY HIGH RESOLUTION NUMERICAL MODELING: A CASE STUDY FOR HAYDARPASA PORT IN THE SEA OF MARMARA

submitted by **BETÜL AYTÖRE** in partial fulfillment of the requirements for the degree of **Master of Science in Civil Engineering Department, Middle East Technical University** by,

Prof. Dr. Gülbin Dural Ünver
Dean, Graduate School of **Natural and Applied Sciences**   _____

Prof. Dr. Ahmet Cevdet Yalçıner
Head of Department, **Civil Engineering**   _____

Prof. Dr. Ahmet Cevdet Yalçıner
Supervisor, **Civil Engineering Department, METU**   _____

Examining Committee Members:

Prof. Dr. Ayşen Ergin
Civil Engineering Department, METU   _____

Prof. Dr. Ahmet Cevdet Yalçıner
Civil Engineering Department, METU   _____

Assoc. Prof. Dr. Utku Kanoğlu
Engineering Sciences Department, METU   _____

Assist. Prof. Dr. Gülizar Özyurt Tarakcıoğlu
Civil Engineering Department, METU   _____

Dr. Cüneyt Baykal
COCONET, EU Project   _____

Date: **26.01.2015**

I hereby declare that all information in this document has been obtained and presented in accordance with academic rules and ethical conduct. I also declare that, as required by these rules and conduct, I have fully cited and referenced all material and results that are not original to this work.

Name, Last name: Betül AYTÖRE

Signature   :

ABSTRACT

ASSESSMENT OF TSUNAMI RESILIENCE OF PORTS BY HIGH
RESOLUTION NUMERICAL MODELING: A CASE STUDY FOR
HAYDARPASA PORT IN THE SEA OF MARMARA

Aytöre, Betül

M.S., Department of Civil Engineering

Supervisor: Prof. Dr. Ahmet Cevdet Yalçıner

January 2015, 93 pages

Assessment of tsunami resilience is used to determine proper mitigation strategies. Thus, it is essential to obtain modeling results in highest confidence and accuracy. Haydarpasa Port in the Sea of Marmara is selected for tsunami assessment study due to vulnerable nature of ports against marine related disasters. The region also tends to have tsunamis since it is located on the western part of the North Anatolian Fault zone where 35 tsunamis occurred in last 2000 years.

The aim of this study is assessment of tsunami resilience of Haydarpasa Port with high resolution models according to most effective submarine earthquake as well as to discuss possible effects of increasing data (actual) and model (numerical) resolution to high level and including existing structures specifically as elevation data. Various numerical computations are performed with tsunami simulation and visualization code NAMI DANCE for this purpose.

The breakwaters are very important for the resilience of Haydarpasa Port. Main requirement to enhance its resilience is to strengthen the breakwaters. Thus, less amplification inside the port and less inundation of port environs can be obtained and

port operations can be continued. Otherwise, such a tsunami will negatively affect this urbanized area by considering economic and social aspects.

The highest model and data resolution lead to most accurate results in tsunami modeling studies. However, resolution of available data is more effective on calculated results in comparison with model resolution. Thus, it is possible to determine a proper model resolution according to needs providing that data resolution is sufficient.

ÖZ

LİMANLARIN TSUNAMİ DAYANIKLILIĞININ YÜKSEK ÇÖZÜNÜRLÜKLÜ SAYISAL MODELLEME İLE DEĞERLENDİRİLMESİ: MARMARA DENİZİ'NDEKİ HAYDARPAŞA LİMANI İÇİN ÖRNEK BİR ÇALIŞMA

Aytöre, Betül

Yüksek Lisans, İnşaat Mühendisliği Bölümü
Tez Yöneticisi: Prof. Dr. Ahmet Cevdet Yalçıner

Ocak 2015, 93 sayfa

Tsunami dayanıklılığı değerlendirmesi, etki hafifletme stratejilerinin belirlenmesi amacıyla kullanılır. Bu nedenle modelleme sonuçlarının en yüksek güvenilirlik ve hassasiyet ile elde edilmesi gereklidir. Marmara Denizi'nde yer alan Haydarpaşa Limanı, limanların denizden gelen felaketlere karşı olan hassas yapıları nedeniyle tsunami değerlendirme çalışması için seçilmiştir. Bu bölge aynı zamanda, son 2000 yıllık zaman içerisinde 35 tsunami meydana gelen Kuzey Anadolu Fay Hattı bölgesinin batı kesiminde yer aldığı için tsunamilere yatkındır.

Bu çalışmanın amacı en etkili deniz dibi depremi kullanılarak Haydarpaşa Limanı'nın tsunamiye dayanıklılığının yüksek çözünürlükle değerlendirilmesi olduğu kadar, veri (gerçek) ve model (sayısal) çözünürlülüğünü yüksek seviyeye çıkarmanın ve binaların yükseklik verisi olarak özellikle ilavesinin olası etkilerini tartışmaktır. Bu amaçla, tsunami benzetim ve görselleştirme kodu olan NAMI DANCE ile çeşitli sayısal hesaplamalar gerçekleştirilmiştir.

Haydarpaşa Limanı'nın dayanıklılığında dalgakıranların önemi büyüktür. Limanın dayanlıklılığını arttırmak için başlıca gereksinim dalgakıranların güçlendirilmesidir.

Böylece liman içinde daha az kabarma ve liman etrafında daha az su baskını sağlanabilir ve liman işlemleri devam ettirilebilir. Aksi takdirde, böyle bir tsunami bu şehirleşmiş alanı sosyal ve ekonomik açıdan olumsuz etkileyecektir.

Tsunami modelleme çalışmalarında, en yüksek model ve veri çözünürlülüğü en hassas sonuçların elde edilmesini sağlar. Ancak, mevcut veri çözünürlülüğünün hesaplanan sonuçlar üzerindeki etkisi model çözünürlülüğü ile karşılaştırıldığında daha fazladır. Bu nedenle, yeterli kalitede veri olduğı sürece ihtiyaca göre uygun bir model çözünürlülüğü belirlenebilir.

<u>Anahtar Kelimeler</u>: Tsunami modellemesi, tsunami değerlendirmesi, Haydarpaşa Limanı, dayanıklılık, yüksek çözünürlük

Dedicated to my well-beloved family…

ACKNOWLEDGEMENTS

I would like to extend my warmest thanks to *Prof. Dr. Ahmet Cevdet Yalçıner* for his everlasting support and assistance to my academic studies and carve out my future. I enjoy every part of my studies in METU Ocean Engineering Research Center, as being the result of his kindhearted and debonair personality and surely his precious experiences.

I would also like to thank *Prof. Dr. Ayşen Ergin* for introducing me the term "coastal engineering", and extend my education with her valuable knowledge and experiences. I always admire her perspective of life and consider myself lucky to have the chance of knowing her.

I would also like to thank *Prof. Dr. Işıkhan Güler, Assist. Prof. Dr. Gülizar Özyurt Tarakcıoğlu*, and *Dr. Cüneyt Baykal* for their strong contribution to my graduate studies and supports.

I dedicate my thanks to *Dr. Andrey Zaitsev* for all his efforts in the modification of numerical code NAMI DANCE used during my research and to *Prof. Dr. Lütfi Suzen* for his helps in GIS environment which is one of the keystones of my study.

When it comes to express my feelings to my well-beloved family, *Mr. Bülend Aytöre, Mrs. Songül Aytöre* and *Mrs. Aytül Karabacak*, words fail. I believe that as long as I have them and sense their support, I can be successful in all areas of my life. I would like to thank them for their endless love, support and patience. I also want to express my sympathies to *Ms. Mira Karabacak* and thank for the joy that she brings to our family.

I would like to thank my associates and friends in METU Ocean Engineering Research Center *Mr. Çağdaş Bilici* and *Mr. Hasan Gökhan Güler,* and my associate and friend in METU *Ms. Nilay İşcen* for their help during my master studies, endless supports and encouragement in all parts of my life and most of all for their elusive patience. My life in the university and even out of the university would be missing without Ms. Nilay

İşcen, and Mr. Çağdaş Bilici particularly. They keep giving me the joy and energy I need in every minute we spend together.

I want to express my deepest gratitude to *Ms. Ceren Çankaya* for her involvement to all parts of my thesis study and my life as a motivator and supporter. She is a ray of sunshine even the hardest times and perfect roommate and holiday partner.

Finally, I would also like to thank my childhood friends *Ms. Gökçe Kübra Turan, Ms. Sinem Madanlar, Mrs. Laçin Erdayı* and *Ms. Dilan Elçi,* and my friends from undergraduate studies at METU *Ms. Begüm Seval, Mr. Görkem Deniz Köksoy* and *Mr. Mert Pülten* for their participation to my graduate studies in some way and understandings and moral supports by any means.

TABLE OF CONTENTS

xiii

LIST OF FIGURES

xv

LIST OF TABLES

LIST OF SYMBOLS

D total water depth

M   discharge flux in x direction

N   discharge flux in y direction

d water depth at the toe of the bottom slope

f friction coefficient

g gravitational acceleration

h water depth with respect to disturbed water level

n Manning's coefficient

t time

u, v depth-averaged water particle velocities in the cross-shore x and long-shore y directions, respectively

η   water surface elevation above still water level

ρ density of sea water

τ_x, τ_y bottom frictions in x and y directions

Ψ   dispersion term

CHAPTER 1

INTRODUCTION

The coastal regions have hosted dense human population throughout history in consequence of high potential of food, transportation and even defense. Today, almost two third of world's population live on the coasts and population density on these regions still grow rapidly. In parallel with the residential value of coastal regions, economic value is also increasing. On the other hand, coastal communities are faced with the risk of water related natural hazards, particularly tsunamis.

Tsunami is a wave or series of waves, which is simply described as displacement of large water volumes by a sudden disturbance of the sea surface. Tsunamis are predominantly originated from submarine seismic activities but even so, volcanic eruptions, landslides, impact of an asteroid and meteorological events might also generate tsunamis. When the world's oceans are considered, the Pacific Ocean region is one of the most prone areas to tsunamis where 52.9% of all tsunamis observed (Bryant, 2008).

Tsunamis are occasional natural hazards in comparison to earthquakes. According to Bryant (2008), only 124 tsunami events recorded among 15,000 occurring earthquakes between the years 1861 and 1948. Correlatively, earthquakes as a more frequent natural hazard have overshadowed the threat of tsunami. However, the importance of tsunamis and tsunami awareness increased in recent decades. After 2004 Indian Ocean and 2011 Great East Japan tsunami events, people began to be more conversant with the term tsunami since these two devastating tsunami events caused a vast number of casualties and loss of property.

Considering revised tsunami catalogue by Altinok et. al. (2011), 134 tsunami events affected Turkish coasts and surroundings in last 3500 years. In the Aegean Sea 51, in

Eastern Mediterranean 41 and in the Sea of Marmara 35 tsunami events occurred from 17th century BC to the recent 1999 Marmara event. In the light of historical documents and prepared databases, it is possible to say that Turkish coasts have tsunamigenic potential. The recent occurrences of catastrophic tsunamis in world's oceans have also raised awareness to tsunamis that might take place around Turkish coasts. Correspondingly, comprehensive studies on preparation of tsunami databases, tsunami hazard analysis and assessments, risk evaluations for the potential tsunami regions and establishing warning systems have accelerated.

Resilience of ports and harbors against tsunamis are essential for proper, efficient and successful rescue operations to reduce the loss of life and property by earthquake, tsunami and marine related disasters (Aytore, 2014). A port is selected as a case study since the trapped tsunami waves inside the ports or enclosed basins lead to strong currents, tend to show resonant amplifications for hours and damage the port components and structures. Hence, the port operations are interrupted. Assessment of those damaging effects of tsunamis inside the harbors is important for the management of post disaster operations. In this thesis, numerical modeling studies are carried out for the Sea of Marmara by focusing on Haydarpasa Port in megacity Istanbul. It is one of the center of economic and commercial activities in Istanbul plus one of the main hubs serving not only cargo handling, but also urban transportation (maritime, railway and highway).

A series of numerical computations are performed by using tsunami simulation and visualization code NAMI DANCE throughout the study. Primarily, effects of various potential tsunamis on the port and its environs are evaluated in order to determine the most damaging one. The rest of the computations are executed according to most effective tsunami for the region to discuss on different resolution conditions in various applications. Therefore, topographic and bathymetric maps of the selected study domains are created by considering different conditions such as data or model resolutions and availability of the existing structures as elevation data. In addition, high resolution modeling (1 m) results are used in tsunami hazard assessment of Haydarpasa Port.

The contents of next chapters in this thesis are summarized as follows: In Chapter 2, previous tsunami studies performed especially for the Sea of Marmara are introduced. In the third chapter, information is given on the chosen modeling tool, NAMI DANCE, with the followed methodology for numerical modeling. Chapter 4 is devoted to the selection of study area, details of available data sets, data processing methods with the tools used for this purpose, and creation of topographic and bathymetric maps for each model. In Chapter 5, historical tsunamis occurred in the Sea of Marmara and, accordingly, tsunami prone areas in the region are summarized. Various simulations are performed by considering tsunami sources that might be affected in Haydarpasa Port in order to identify the most critical source for the port in terms of inundation extents and tsunami heights. The most critical source is used in the following modeling studies. The procedure related to inputting the selected source mechanism in NAMI DANCE is also clarified in this chapter. The simulation results of each model are presented in Chapter 6. The obtained results are discussed in Chapter 7 by considering the possible effects of changing data (actual) and model (numerical) resolutions. In addition, estimated tsunami wave impact on the port and its environs as well as tsunami assessment strategies for the region are discussed in the same chapter. Finally, Chapter 8 concludes this study with the suggestions on future studies.

CHAPTER 2

LITERATURE SURVEY

Numerous studies on tsunami modeling by using different processing and computational techniques to see the effects of different levels of tsunamis are available in the literature. Here in this section, a broad information about some selected studies related to tsunami potential of Turkey especially focusing on the Sea of Marmara, tsunami inundation analysis around Turkey, various parameters that have influence on inundation characteristics and different tsunami modeling techniques are given.

Altınok et. al. (2011) revised available past catalogues, literature papers and geophysical data and, presents the most recent tsunami catalogue affected on Turkish coasts based on the definitions given in two different EU projects, GITEC (Genesis and Impact of Tsunamis on the European Coasts) and TRANSFER (Tsunami Risk And Strategies For the European Region). Among the 134 tsunamigenic events, which occurred between the years 1410 BC and 2000, listed in the study, 35 events took place in the Sea of Marmara. However, as being the result of difficulty in determination of source locations and mechanisms of past events, only 4 events out of 35 have sufficient information to be used in assessment studies. In the study, it is also indicated that tsunamis caused by slope failures also occurred in the Sea of Marmara and some of those triggered during major earthquakes.

Papadopoulos et. al. (2014) studied geological signatures, generation mechanisms and coastal impacts of historical and pre-historical tsunamis in the Mediterranean and its connected seas. The authors presented a newly revised map of 22 tsunamigenic zones with tsunami generation potentials. According to authors, the eastern side of the Marmara Sea is one the most important tsunamigenic zones in the selected region. The mean tsunami reoccurrence in the Marmara Sea estimated as 500 years in the study.

The authors indicated that there is noteworthy tsunami risk for coastal zones of Mediterranean and its connected seas.

Necmioğlu and Ozel (2014) studied relationship between earthquake source parameters and tsunami propagation by focusing on the Eastern Mediterranean. In the article, the difficulty in determining earthquake parameters, especially where complex tectonics occur, is mentioned. According to sensitivity analysis on this relationship performed in this study, it is seen that strike and rake variation strongly affects tsunami generation. Therefore, it is an option to consider these parameters due to determine the worst case scenario that will be used in tsunami hazard studies. Authors also recommended conducting sensitivity analysis for selected region to determine earthquake parameters which led to maximum tsunami generation.

Dilmen et. al. (2014) performed tsunami simulation and inundation assessment for the Gulf of Fethiye and developed a tsunami inundation map for the region in their study. High resolution bathymetry and topography dataset with 3 m used and 14 probable tsunami scenario considered for inundation mapping. A worst-case tsunami scenario is selected according to wave amplitudes and maximum tsunami flow depths in the Fethiye Bay and quantitative tsunami inundation map is presented in the study. According to results, lowland near shore regions with low land topography are likely to have significant inundation. Areas along those regions are highly populated which increase the potential tsunami damage. Dilmen also claims that presence of Sovalye Island located in front of the bay, partly prevents entering tsunami waves but it keeps the energy inside the bay at the same time and causes more agitation. Dilmen (2009), also studied Fethiye Bay in Turkey and Kiparissia-Zakintos-Pylos in Greece by preparing GIS based tsunami inundation maps in her thesis. The author remarked that appending the heights of the buildings to topography results with decreasing propagation of tsunami waves to the inland areas.

Yalciner et. al. (2014) conducted a study at the Northwest Nile Delta in Mediterranean Sea based on a hypothetical landslide scenario followed by tsunami. Two different models, TWO LAYER (Imamura and Imteaz, 1995; Yalciner et al., 2002) and NAMI DANCE, used in the study for landslide generation, and tsunami propagation and

6

inundation, respectively. The authors indicate that Eastern Mediterranean is a semi-enclosed region and this causes tsunami wave reflections, which are responsible for occurring of largest wave in the second wave train.

Yalciner et. al. (2014) performed a tsunami modeling study, which focus on western part of Peloponnese in Greece, in the framework of EU SEAHELLARC project. In the study, the characteristics of possible tsunami sources for the region are determined. The most effective ones on selected coasts, Pylos, Kyparissia, Filiatra and Zakynthos are identified and relevant simulation results are presented to estimate tsunami risk in those areas.

Hébert et. al. (2004) discussed active faults in the Marmara Sea and possible impacts of a tsunami hazard on Istanbul Coasts. The area focused in the study also contains smallest study domain chosen in this thesis, where Haydarpasa Port is in. However, model resolution used in the article is 20 m. Hébert studied three probable earthquake sources on NAF zone and submarine landslide sources affected on the region. According to results presented, earthquakes in the Eastern Marmara Sea is more effective on Istanbul coasts in comparison to earthquakes in Western basin. However, possible damage caused by landslide-generated tsunamis is higher. In the article, it is also mentioned that tsunami waves generated by submarine earthquakes reach Istanbul coasts within 5 to 10 minutes and run-up heights are around 2 m. Historical documents and water depths in Marmara region show that run-ups greater than 10 m is not expected around Marmara coasts.

Zitter et. al. (2012) worked on the slope instabilities in the Sea of Marmara. The focus of the study was the submarine mass wasting in the region, with their distributions, triggering factors and morphological relations. Submarine slope failures and mass wasting deposits are identified, mapped and dated in the study. It is determined that mass wasting features in the Sea of Marmara are very common, since the region enables very suitable conditions, and about 30% of them are submarine mass movements. The study points out that trigger mechanisms of slope instabilities are affected by the distribution of crustal stress and strain, paleo environmental conditions and sea-level change.

Insel (2009) examined the effects of landslide parameters, mainly density and thickness of the slid material, on the tsunami wave generation by selecting a case study region, Yalova in the Sea of Marmara. The author noted the existing tsunami potential of this region by considering the active fault zones. In the study, it is comprehended that higher densities and thicknesses of slide material cause higher water surface elevations.

Aydin (2014) also studied tsunami generated by submarine landslides in the Marmara Sea. The author emphasized on the hazardous nature of Marmara Sea coasts in point of tsunami generated by submarine landslides. In addition, a linear relation between slide thickness and velocity observed and the effect of slide velocity on tsunami wave generation discussed in the study.

Ayca (2012) studied on six different tsunami scenario in the Sea of Marmara, and presented the results for each case in 90 m resolution. He concluded in his thesis that Prince's Islands Normal (PIN) is the most critical scenario for Istanbul. However, the maximum and minimum wave amplitudes obtained from the gauge located at Haydarpasa given in the study are 1.4 m and -4.5 m for PIN and 2.3 m and -2.6 m for Yalova Fault Normal (YAN), respectively. Therefore, it is tentatively possible to say that YAN scenario is more critical at the specified region, Haydarpasa. He also developed of a web GIS-based tsunami inundation mapping for Marmara Sea Region.

Kaiser et. el. (2011) presented a case study in Phang Nga and Phuket in Thailand after 2004 Indian Ocean tsunami that provides comprehensive information about land cover roughness and built environment influence on inundation characteristics. The topographic and bathymetric maps used in the analysis have 1 m resolution. The wave series obtained from nested study domains with larger grid sizes are used for high resolution simulations to reduce long computation time. In addition, obtained results are compared with field observations. In the study, it is concluded that mangroves may reduce current speed by half while there is nearly no change observed on inundation extent. However, if buildings are not included in the model, a significant overestimation of the inundation extent occurs.

Pamuk (2014) conducted a similar study with Kaiser. The author investigated influence of buildings and roughness coefficient on tsunami motion in inundation zone by comparing 5 different simulations performed for Belek region in Antalya. In the study, tsunami analysis with high resolution bathymetry and topography is recommended for residential areas to obtain accurate and reliable velocities and inundation depths. It is stated that including friction reduces the inundation distances and discharge fluxes observed in the selected region. To identify possible morphological changes due to tsunami attack, a non-dimensional parameter Rouse is also interpreted in the study.

Onat (2011) prepared a database and applied to Eastern Mediterranean for tsunami warning system in her thesis. The effects of certain source parameters (dip and rake angles) are discussed in the study. According to tsunami modeling results obtained for selected study area, higher tsunami waves are observed when dip angle is decreasing and rake angle is increasing. Since these parameters affect the results, better estimation of tsunami source parameters are highly important. Onat and Yalciner also published an article on the same topic in 2013. In the article it is pointed out that, a practicable tsunami-warning system requires a preparation of tsunami dataset as well as increasing public awareness and developing mitigation strategies.

Ozel et. al. (2011) informed about the historically and instrumentally recorded tsunamis around Turkey to have a better understanding of tsunami potential of the region. Modeling results from selected tsunamigenic regions, Rhodes and SW of Turkey, are also included. In the article, it is also mentioned that Kandilli Observatory and Earthquake Research Institute (KOERI) has started to install 5 sea floor observation systems in the Sea of Marmara to increase their observational capabilities and to surely reduce the early warning time and the minimum magnitude threshold down to 1.0 in the Marmara Sea in case of a possible tsunami. The short arrival times in the Marmara and Aegean Seas are underlined and importance of establishment of a Tsunami Warning Center in Turkey is repeated.

Ozdemir (2014) developed a simple and high-speed informative tsunami warning system for Marmara coasts his thesis. A series of simulations are performed by using

previously determined seismic sources in the Sea of Marmara in NAMI DANCE for the data base. The related results are also presented and discussed in the study. According to presented results, expected maximum tsunami wave height at a gauge selected near Haydarpasa is around 1 to 2 m. However, the resolution of the model used in study is 90 m.

CHAPTER 3

NUMERICAL MODELING

The chosen numerical tool for modeling and its capabilities, information on long wave theory and the followed methodology that shows general phases of tsunami modeling study are included in this chapter.

3.1. Brief Information on Modeling and Numerical Code NAMI DANCE

Numerical modeling, which is simply for a better understanding of the effect of tsunamis by considering bathymetric and topographical condition, plays an important role in both scientific and operational tsunami studies for better preparedness, wider awareness and determination of proper mitigation strategies. In the simplest term, tsunami modeling phases are creation of bathymetric and topographic maps in sufficient resolution for previously specified region according to the needs, comparison of possible tsunami sources that might be affected in the region to determine the most effective source and, application of the validated and verified numerical tools to observe tsunami generation, propagation and inundation to be used in assessment studies.

There are many different numerical models used to make tsunami predictions both for academic and operational purposes. The widely used numerical models among these are COMCOT (Liu et al, 1994; 2008), TUNAMI-N2 (Imamura, 1996) and MOST (Titov and Synolakis, 1998).

The numerical model NAMI DANCE is selected and used throughout this thesis. It is a computational tool developed in collaboration with Middle East Technical University and Russian Academy of Science by the scientists Andrey Zaytsev, Ahmet Yalciner, Anton Chernov, Efim Pelinovsky and Andrey Kurkin, particularly for tsunami simulation and visualization (NAMI DANCE, 2011).

NAMI DANCE has been developed in C++ programming using the same computational procedures of TUNAMI N2, which computes all necessary parameters of tsunami behavior both in shallow water and in the inundation zone including computation of tsunami source characteristics from earthquake rupture characteristics (rupture source input). Addition to these, NAMI DANCE can provide solution in nested study domains with the selection of calculation type and system, which are nonlinear or linear forms of Cartesian and spherical shallow water equations, determined previously by the user.

To explain briefly, NAMI DANCE calculates maximum and minimum water surface elevations, current velocities and their directions, momentum fluxes and their directions, flow depths, hydrodynamic forces and Froude number in selected study domain or nested domains by using beforehand user defined output time intervals and durations. Besides, initial tsunami wave motion can be created by using time series of water surface fluctuation inputted arbitrarily (border source input), as well as using available tsunamigenic rupture parameters of earthquake or user defined dimensions and shapes of the surface disturbance (rupture source input) (Ozer, 2012).

There are some additional features in NAMI DANCE to visualize the computed tsunami parameters. One of them is the tool to create 3D plots in selected time interval with an option of defining multiplier of topography, wave amplitude, bathymetry and truncation of land topography to enhance the visual appearance in selected domain, and controlling the camera position and lights to be able focus on a specific area. It is also possible to create animations by using prepared 3D plots for tracing the tsunami wave motion and inundation.

In the final version of NAMI DANCE, it is also possible to choose the number of processors of executed computer to be able to increase the speed of the simulations or increase the available processor number to use in other tools and decrease the loss of time for the user that works with multiple computer tools.

3.2. Theoretical Background

Numerical modeling tools solve similar long wave equations for tsunamis with different approach techniques to the problem in general. This difference results in change of computer time and memory, and error limit.

NAMI DANCE solves Nonlinear Shallow Water (NSW) Equations with respect to related initial and boundary conditions, since using these equations consumes reasonable computer time and memory with results in acceptable error limit.

The Shallow Water Theory is derived from the Navier-Stokes Equations for conservation of mass and momentum in two-dimensional unsteady solution. The vertical component of water particle acceleration in z direction is negligible in these equations when it is compared with gravitational acceleration in x and y direction (Ozer, 2012). After boundary conditions at the sea surface and bottom are applied, the two-dimensional Shallow Water Equations including dispersion terms become:

$$\frac{\partial \eta}{\partial t} + \frac{\partial M}{\partial x} + \frac{\partial N}{\partial y} = 0 \qquad\qquad [3.1]$$

$$\frac{\partial M}{\partial t} + \frac{\partial}{\partial x}\left(\frac{M^2}{d}\right) + \frac{\partial}{\partial y}\left(\frac{MN}{d}\right) + gd\frac{\partial \eta}{\partial x} + \frac{\tau_x}{\rho} = \frac{\partial \psi}{\partial x} \qquad\qquad [3.2]$$

$$\frac{\partial N}{\partial t} + \frac{\partial}{\partial x}\left(\frac{MN}{d}\right) + \frac{\partial}{\partial y}\left(\frac{N^2}{d}\right) + gd\frac{\partial \eta}{\partial y} + \frac{\tau_y}{\rho} = \frac{\partial \psi}{\partial y} \qquad\qquad [3.3]$$

In these equations, x and y are the axes of Cartesian coordinate, t is time, η is water surface elevation above still water level up to free surface, and M and N are the discharge fluxes in the x and y directions which are also defined in the equations below:

$$M = \int_{-b}^{\eta} u\,dz = u(d+\eta) = ud \,, \quad N = \int_{-b}^{\eta} v\,dz = v(d+\eta) = vd \qquad [3.4]$$

The other parameters u and v are current velocities in x and y directions, g is gravitational acceleration, ρ is the water density, D is total water depth (D=d+η), τ_x and τ_y are the bottom shear stress in x and y directions. The bottom shear stresses,

which are defined in following equations, are generally correlated with bottom friction, f.

$$\frac{\tau_x}{\rho} = \frac{fn^2}{D^{7/3}} M \sqrt{M^2 + N^2}$$ [3.5]

$$\frac{\tau_y}{\rho} = \frac{fn^2}{D^{7/3}} N \sqrt{M^2 + N^2}$$ [3.6]

In these equations, n represents Manning's coefficient and it is expressed as follows:

$$n = \sqrt{\frac{fD^{1/3}}{2g}}$$ [3.7]

Finally, the dispersion terms are defined in the equations given below:

$$\psi = \frac{h^2}{3} \left(\frac{\partial^2 u}{\partial x \partial t} + \frac{\partial^2 v}{\partial y \partial t} \right)$$ [3.8]

where h is water depth with respect to disturbed water level.

It is important to mention that the version of NAMI DANCE used in this thesis solves nonlinear form of Shallow Water Equations without dispersion term.

In addition, some hydrodynamic parameters are (water surface elevation, flow depth, run-up and inundation distance) in tsunami inundation zone are shown in Figure 3.1. One of the most important parameter of this study is inundation distance. It is the horizontal distance between original shoreline and inundation border. Correspondingly, tsunami run-up is the elevation of the inundation border with respect to still water level and flow depth is the height of water surface from the ground.

14
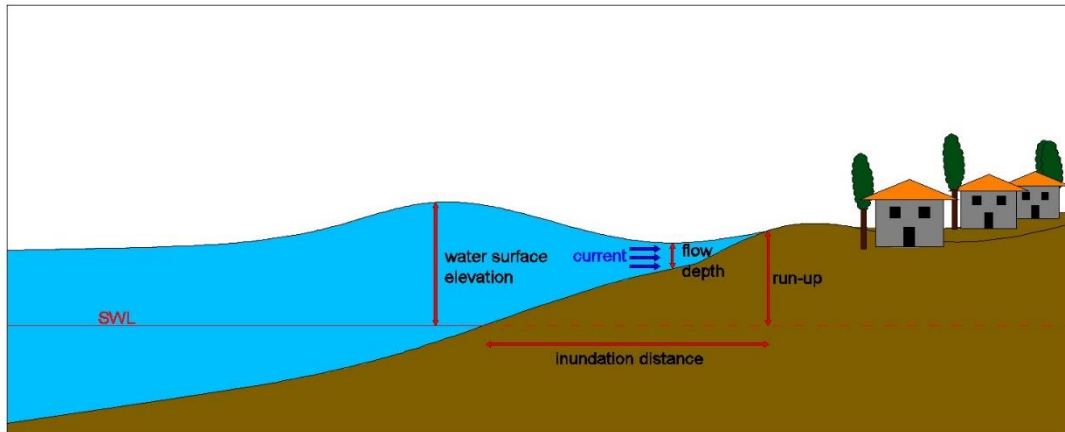
Figure 3.1. Hydrodynamic parameters in inundation zone

3.3. Methodology

In general, method of tsunami modeling used in this study has five phases that are selection of the study area, data acquisition and processing, creation of bathymetric and topographic maps and placing gauges, selection of the tsunami source and finally, tsunami analysis by using NAMI DANCE. The details of method of numerical modeling with the code NAMI DANCE is given in Figure 3.2.

1. SELECTION OF THE STUDY AREA

• Review of available data sources
• Select a study area by considering all possible aspects including:
  • tsunami and earthquake potential of the region,
  • importance of the region in population and industrialization point of view,
  • nature of available structures etc.

2. DATA ACQUISITION AND PROCESSING

• Collection of data from different sources for selected area
• Data management
  • Data analyzing
  • Data elimination
• Data conversion
• Data processing
• Additional digitization

3. CREATION OF BATHYMETRIC AND TOPOGRAPHIC MAPS AND PLACING GAUGES

• Determination of each study domain and their resolution
• Creation of the maps
• Place gauges at important locations to track the tsunami wave motion

4. SELECTION OF THE TSUNAMI SOURCE

• Collect information on historical earthquakes and tsunamis occurred in the selected region
• Estimation of possible tsunami sources
• Comparison of the sources to determine the most effective source for the region
• Creation of the source according to computed tsunami source parameters by considering its implementation in the code (NAMI DANCE) such as:
  • Rupture source input
  • Border source input (time series of water surface fluctuation)

5. TSUNAMI ANALYSIS BY USING NAMI DANCE

• Determination of some basic parameters to be used in the simulations such as:
  • duration of the simulations according to arrival time of waves to the selected area
  • output time interval by considering speed and memory limitations
  • time step according to limits calculated by the code
  • friction coefficient
• Visualization of the results after the end of simulations by:
  • inundation mapping
  • presenting summary result tables
  • drawing graphs
  • creating animations

Figure 3.2. The flow chart of the methodology followed in the study

CHAPTER 4

DATA ACQUISITION AND PROCESSING

This chapter covers the detailed information on the selected study area and data used in different parts of the study with formats and characteristics of available data. The processing details of obtained data and computational tools used for this purpose during the study are included in this chapter.

4.1. Selected Study Area

Istanbul, located in the Marmara Region in northwestern part of Turkey, is the most populated city in the country and in Europe with over 14 million people (Turkish Statistical Institute, 2014). The transcontinental city has a great importance with its strategic location on the Bosphorus strait and its invaluable historical assets that goes back more than 300 thousand years (Istanbul Metropolitan Municipality, 2009). In addition, Istanbul plays a role as the industrial and commercial center of Turkey.
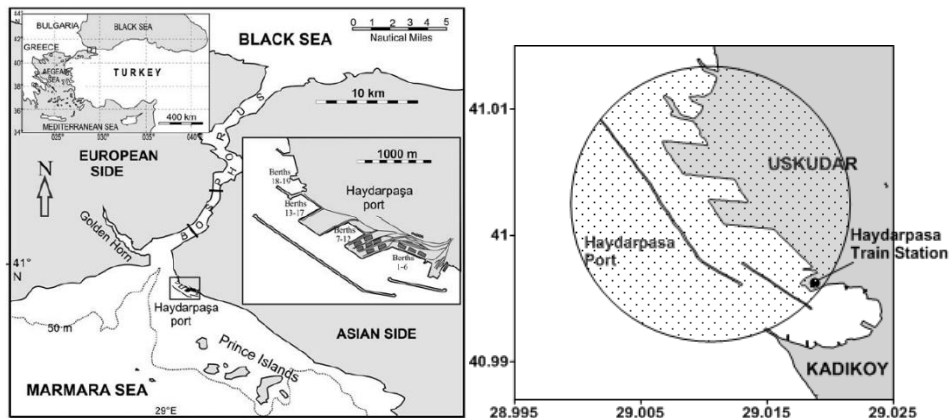
Figure 4.1. Location of the Haydarpasa Port (by Ünlü, 2007) on the left and selected smallest study domain on the right

Corresponding to economic significance of Istanbul, the city possess several commercial ports. The selected area in this study also hosts an important port, known as Haydarpasa Port. The port is the oldest and the largest container port in the Marmara Region and third largest in the nation. The port and its environs are placed in between two counties, which are the two of the populous counties among the thirty-two, Kadikoy and Uskudar in Anatolian side of Istanbul (Istanbul Metropolitan Municipality, 2009). The location and general view of the port with its components are given in Figure 4.1 and Figure 4.2, respectively. The two breakwaters of the port seen in the figure are about 1,700 and 600 m long and, General Directorate of Turkish State Railways (TCDD) operates the port. The handling and storing general cargo and container, ro-ro handlings, and short/long distance passenger transfers are the components of the port in general (Yalciner et. al., 2014).

International and domestic maritime transportation is extensively observed in Istanbul. Therefore, intensity of maritime traffic is very high in Bosporus. As being an alternative to the bridges, the connection of two peninsulas are also provided by the ferries. One of the main docks in Asian side is Kadikoy Ferry Terminal located in the selected study area. In addition, entrance of Haydarpasa-Gebze Railway Line, which is under construction as being one of the extensions of Marmaray Project, is in this selected region.

Figure 4.2. A view of selected region on the left and Haydarpasa Train Station on the right (Istanbul Metropolitan Municipality, 2007 and 2014)

Moreover, selected study region hosts a historic train station goes by the name of Haydarpasa Train Station (Figure 4.1 and 4.2). It is completed in 1908 during the Ottoman Empire in order to build an enchanting exit to the beginning of Baghdad Railway Line. It is the first gateway of Istanbul to Anatolia and Middle East (Safak, 2010). Haydarpasa Train Station is one of the spectacular monuments that suits the historical landscape of Istanbul. Today, modernization process of the old station to become the terminal of high-speed services between Istanbul and Ankara is in the planning stage.

On the other hand, Marmara Region is a tectonically active zone since it is located on North Anatolian Fault (NAF). Numerous catastrophic events mainly like earthquakes or earthquake/landslide induced tsunamis occurred in the Marmara Sea basin and may continue to occur in the future. As indicated above, many of the historical, industrial and commercial structures are situated near coastal areas of Istanbul. Therefore, water generated impacts in particular to tsunamis should be carefully investigated since these impacts can create excessive damage especially on the ports as a consequence of their vulnerability against such forces. These impacts may cause not just loss of life but also loss of property results in negative economic effect in the region and even country. For this reason, Haydarpasa Port area is selected as the case study for tsunami assessment in this thesis.

4.2. Sources of Bathymetry, Shoreline and Topographical Data

The available dataset, which is used in order to create topographic and bathymetric maps of chosen domains, is very critical in tsunami modeling studies. The more detailed and precise dataset contributes to obtain more reliable inundation maps and other calculated tsunami parameters to be applied in mitigation strategies. In this study, different data types are gathered for this purpose if overall is considered.

Bathymetric and Shoreline Data

The bathymetric data is acquired from General Bathymetric Chart of the Oceans (GEBCO) of the British Oceanographic Data Centre. GEBCO provides public available bathymetric grid sets for world's oceans with a spatial resolution of 30 arc-

seconds in general. The bathymetric information of GEBCO is mainly generated from a database of ship-track soundings with interpolation between soundings guided by satellite-derived gravity data (General Bathymetric Chart of the Oceans GEBCO_08 Grid, 2010). It contains digitized current GEBCO GDA contours, GLOBE land elevations, WVS coastlines, SCAR (Antarctic) coastlines, additional shallow-water contours and soundings, additional intermediate contours in featureless areas and, additional individual echo-soundings. Thus, to form each model's bathymetric map, data from GEBCO is used.

Nevertheless, the dataset obtained from navigational charts is added to improve bathymetric data in high resolution maps since GEBCO is insufficient in shallow water regions, especially inside the port area due to its resolution. Besides, images from Google Earth are used to define a better shoreline and location of the breakwaters in the chosen domain. The cross-section of breakwaters of Haydarpasa Port are acquired from technical drawings used in construction of the breakwaters.

Topographic Data

Topographical data is acquired from different sources for each model. In the first model, topographical data is downloaded from LP DAAC Global Data Explorer that provides the Advanced Spaceborne Thermal Emission and Reflection Radiometer (ASTER) Global Digital Elevation Model Version 2 (GDEM V2) for online users. ASTER is one of the five remote sensors on board NASA's Terra satellite that collects multispectral images. It provides data with 15 to 90 meters spatial resolution. These images have been used to produce digital elevation models with vertical accuracies between 10m and 25m. ASTER GDEM is a 1 arc-second elevation grid distributed as 1°x1° (ASTER GDEM V2, 2011).

For all models except the first one, the topographical data purchased from Directorate of Cartography underneath of Department of Housing and Urban Development of Istanbul Metropolitan Municipality (IMM) are used to be able to create higher resolution topographic models for selected region in comparison with ASTER GDEM.

In general, the purchased data from IMM has two parts: one is the raster data of digital elevation models that covers all counties of Istanbul and second is different vector data (points, lines and polygons) related to all type of structures in all counties of Istanbul. The available data is produced by using orthophoto technique. The resolutions of DEMs and vector data are 5 m and 1 m, respectively. In Figure 4.3, view of DEMs for Uskudar and Kadikoy counties with a red rectangle indicating smallest study domain is given.
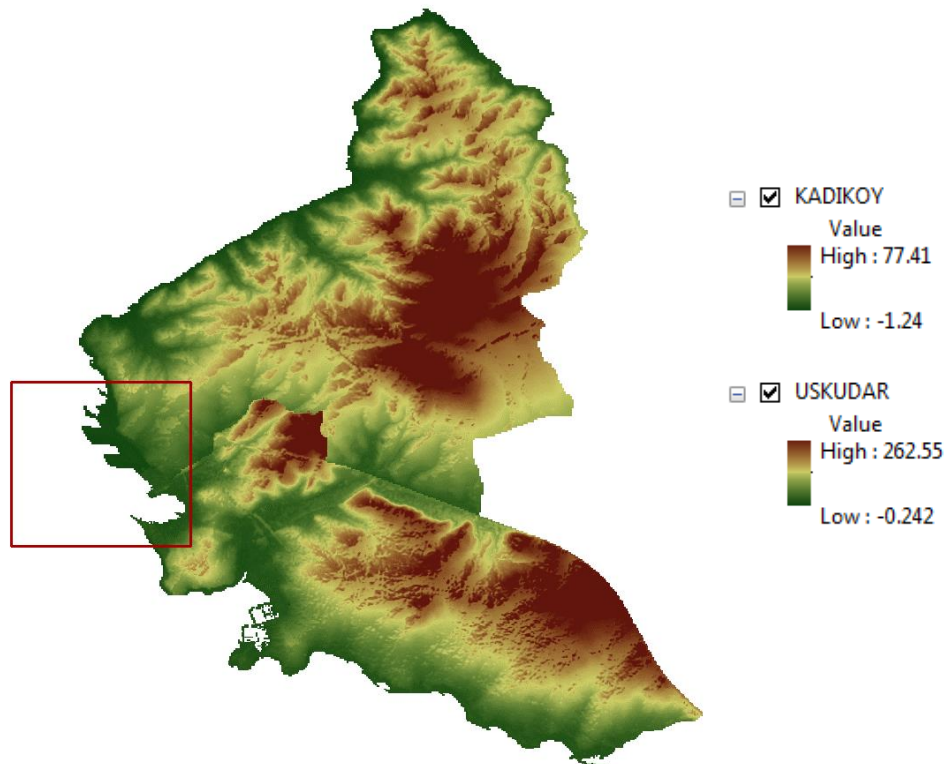
Figure 4.3. The view of available DEMs for both Uskudar and Kadikoy region with indicating the smallest domain

Available polygon vector data mainly covers different type of structures. In Figure 4.4, list of available polygon data and view of polygon structures for Uskudar and Kadikoy counties is given. In addition, polygon structures in the smallest domain includes Haydarpasa Port is available to have a better view in the same figure. There are 29 different polygon layers in Uskudar. Those are, stairs, religious building, greenhouse, transformer, fountain, building under construction, commercial building, well, water

tank, official building, oil tank, gas station, manufacturing building, terrace, pool, school, pylon, road skid, ruins, shelter, temporal lake, closed bus-stop, load control platform, residential building, loading platform, factory chimney, factory, sport facility and cesspool according to order in the list. There are also 27 different polygon layers in Kadikoy, which are nearly same as the ones in Uskudar.
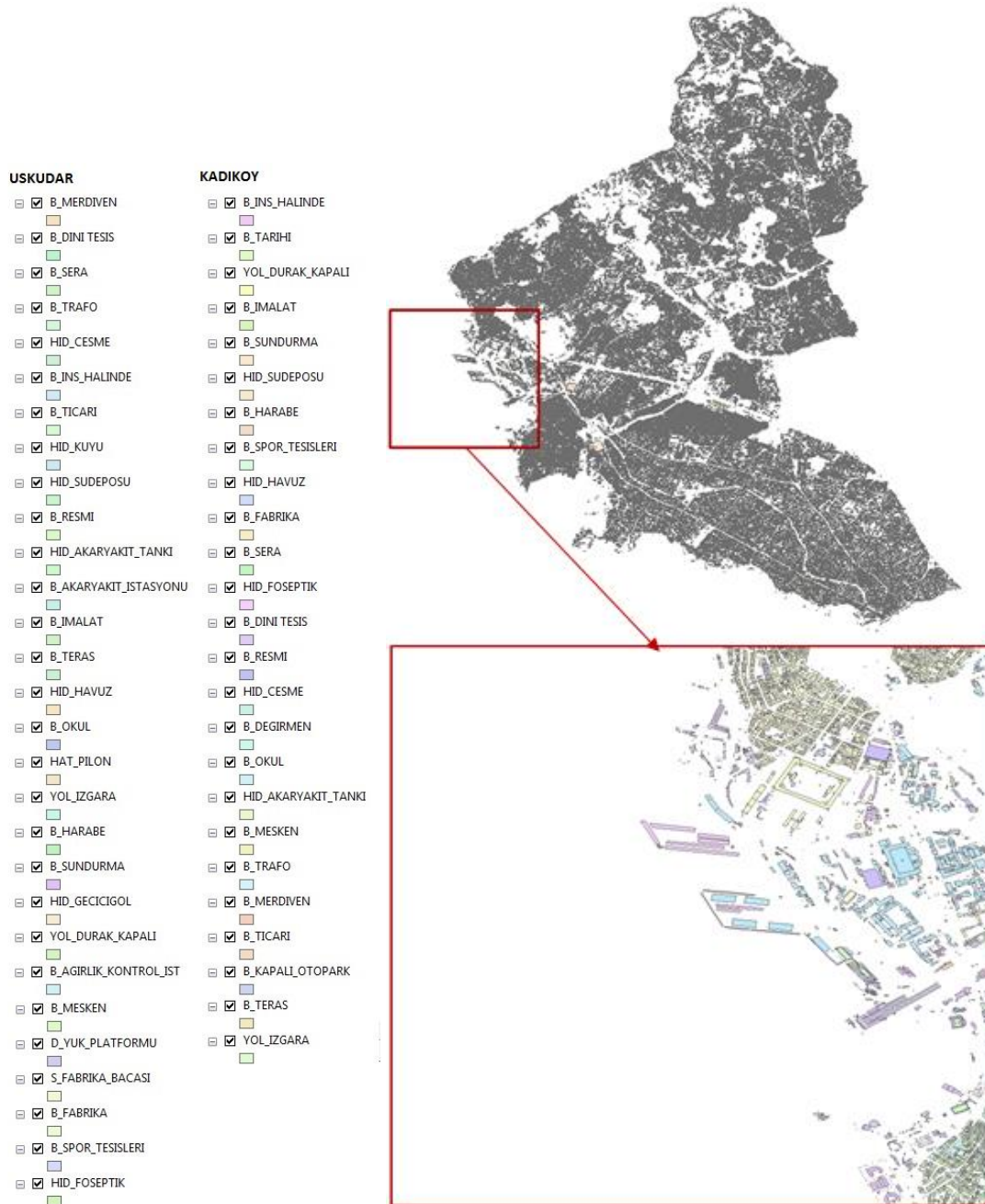
Figure 4.4. The list and view of available polygon layers both in Uskudar and Kadikoy region, and polygon layers available in the smallest domain

22

Each polygon layer has different attribute tables that consists of each object's value, shape and location information. Elevation, external surface and spatial information of objects are crucial to create high resolution topographic maps in this study.

Available point vector data is not that crucial since point data mainly covers point structures such as lighting post, bush, sculpture etc., which are not effective as polygon objects when it comes to their resistance against tsunami forces.

Existing line data is already covered in raster data. Nevertheless, some selected line layers are used during the data processing of high resolution maps. The list of selected line layers in the smallest domain and a view of those layers are given in Figure 4.5. There are 7 different line layers in Uskudar. Those are retaining wall, two sided partition wall, one sided partition wall, pier, dock, railway and roadway and, 11 different line layers in Kadikoy as pier, breakwater, retaining wall, dried brook, one sided partition wall, roadway, lake, two sided partition wall, cark park, walking track and dock according to order in the given list.

Figure 4.5. The list and view of used line layers both in Uskudar and Kadikoy region

4.3. Data Management, Processing and Digitization

Data management, processing and digitization to develop bathymetric and topographic models, especially shoreline position, of the study region in highest resolution by using the data stated in the Section 4.2 is one of the most challenging parts of tsunami analysis.

For data management, processing and digitization, different computational tools have been used. These tools are listed below:

- **ArcGIS 10.0©:** It is a geography platform to collect, store, manipulate and display spatial information in general terms. Almost in every step of data management from visualization of data is to be managed to preparation of final topographic and bathymetric maps in this study, this tool have been used.

- **MATLAB 2010©:** It is a high performance tool for numerical computation, data analysis and visualization in general terms. With the help of this tool, the needed data processing in some parts of the study, especially data organizing and scrubbing, is performed.

- **Microsoft Visual Studio 2008©:** It is an integrated development environment. During the study, it is mainly used for data scrubbing like MATLAB.

- **Surfer 12©:** It is a tool for contouring, gridding, and surface mapping. During the study, maps are displayed and enhanced in Surfer 12. Additional digitization is also performed in this program.

4.3.1. Data Conversion

The coordinate system of all data has been used is converted into same coordinate system which is geographic coordinate system, GCS_WGS_84 since this coordinate system is supported by tsunami modeling software NAMI DANCE.

The database of GEBCO and ASTER is stored as GCS_WGS_84. Therefore, there is no need for conversion of data obtained from their database. The original projection system of dataset acquired from Istanbul Metropolitan Municipality is assigned as ITRF96_UTM_ZONE_35 with the given projection properties in Table 4.1. The data

in this projected coordinate system is converted into GCS_WGS84. All necessary data conversions are performed by using ArcGIS 10.0.

Table 4.1. Properties of projection of data from IMM (ITRF_96_UTM_Zone_35N)

Projection	Transverse Mercator
False Easting	500000.0
False Northing	0.0
Central Meridian	30.0
Scale Factor	1.0
Latitude of Origin	0.0
Linear Unit	Meter (1.0)
Geographic Coordinate System	**GCS_GRS_1980**
Angular Unit	Degree (0.0174532925199433)
Prime Meridian	Greenwich (0.0)
Datum	D_ITRF_1996
Spheroid	GRS_1980

4.3.2. Data Processing

To manage all, each available dataset is converted to xyz (longitude, latitude and elevation) format as data file. The data from ASTER, GEBCO and DEMs from IMM is in raster format. Thus, these datasets are easily converted and saved as data file. Merely, since there is no available data for water bodies in ASTER, it automatically assigns "0" at those locations. After ASTER data converted to data file, these zero values are eliminated with the help of MATLAB and Visual Studio Intel Fortran.

For the available polygon vector data, different procedure for managing data is followed. First, minimum 200 different points, where the number changes according to size of structures available on that data set, are assigned in each polygon in a layer with an add-on named as ET GeoWizard for ArcGIS. By following this procedure, it is expected to be able to identify each building on the high resolution maps. Addition to assigning points inside each polygon, new points are assigned on the vertices of each polygon to keep their shape information as much as possible. All points with spatial location and elevation information are stored in data files. The available selected line features are also converted to multiple point features and all those points stored in data files with spatial location and elevation information.

If every structure on the high resolution map is identified clearly, i.e. every building rises up as they are in real life, tsunami waves are supposed to show different propagation when they face with a structure that resists. Therefore, the change in inundation map is expected in tsunami analysis section.

In NAMI DANCE, elevations of bathymetric and topographic data are defined with positive and negative signs, respectively. When all data is converted to data file, elevations of topographic data obtained from GEBCO, ASTER and IMM are multiplied by -1 for compatibility with NAMI DANCE.

The available bathymetric map that belongs to the study region is placed on its spatial location and digitization has been performed. Consequently, the resolution of bathymetric data increased.

After storing all required data for each model in single data files, the regularly spaced data points of each model's domains are computed for the input of numerical tool by using Surfer-12. During interpolation of data to obtain these regularly spaced data points (gridded maps), Kriging method was preferred. Kriging solves a set of linear equations to fit a function by using values at nearby locations and predict the best output value at an unknown point. In other words, Kriging is an interpolation method, which is generally used in geostatistics. The main reason of using this method to create the gridded maps is its ability to provide unbiased estimates with minimum variance where it differs from other deterministic interpolation methods (Oliver and Webster, 2014).

4.3.3. Additional Digitization

After processing of all available data that is needed for each model, gridded bathymetric and topographic maps are created with chosen grid sizes. However, to finalize those maps, some additional digitization is required especially for the ones with larger grid sizes. For this reason, the quality of raster maps obtained for each model is also checked by comparing maps with aerial photography. Manual adjustment (fine-tuning) is applied to necessary models to reflect the coastal topography of the chosen domain more accurately.

The one of the most important structures that will resist tsunami waves are breakwaters. By using the acquired cross-section data from technical drawings used in construction, two breakwaters that belong to Haydarpasa Port have been digitized.

4.4. Created Bathymetric and Topographic Maps

In this section, bathymetric and topographic maps for each model are given with related study domains and their grid sizes used in the tsunami analysis. Different analyses have been performed by using different models in NAMI DANCE to compare their results considering various aspects such as effects of increasing data and model resolutions. In addition, different models are used since there need to be some changes in the followed procedure during source implementation, which will be explained in detail in Section 5.3.

4.4.1. Bathymetric and Topographic Map of Model 1

Bathymetric and topographic maps of Model 1 are created by using ASTER and GEBCO data and performing additional digitization like it is explained in Section 4.2 and 4.3. In other words, maps of Model 1 are created by using general procedure followed in tsunami analysis studies when there is no additional data available.

The tsunami analysis of this first model is performed by using nested study domains. The grid size of largest domain named Domain B is chosen as 90 m. According to the principal of nested analyses in NAMI DANCE, the boundary of smaller domain should involve in the previous larger domain and the smaller domain should have one-third grid size of the previous larger domain. Because of this principal, the grid sizes of Domains C and D are stated as 30 m and 10 m, respectively. The general view of the nested study domains B, C and D are given in Figure 4.6. The red rectangles inside the larger domains indicate the location of next smaller domain inside. Table 4.2 summarizes the nested study domains of Model 1 with their boundary coordinates and grid sizes.

27
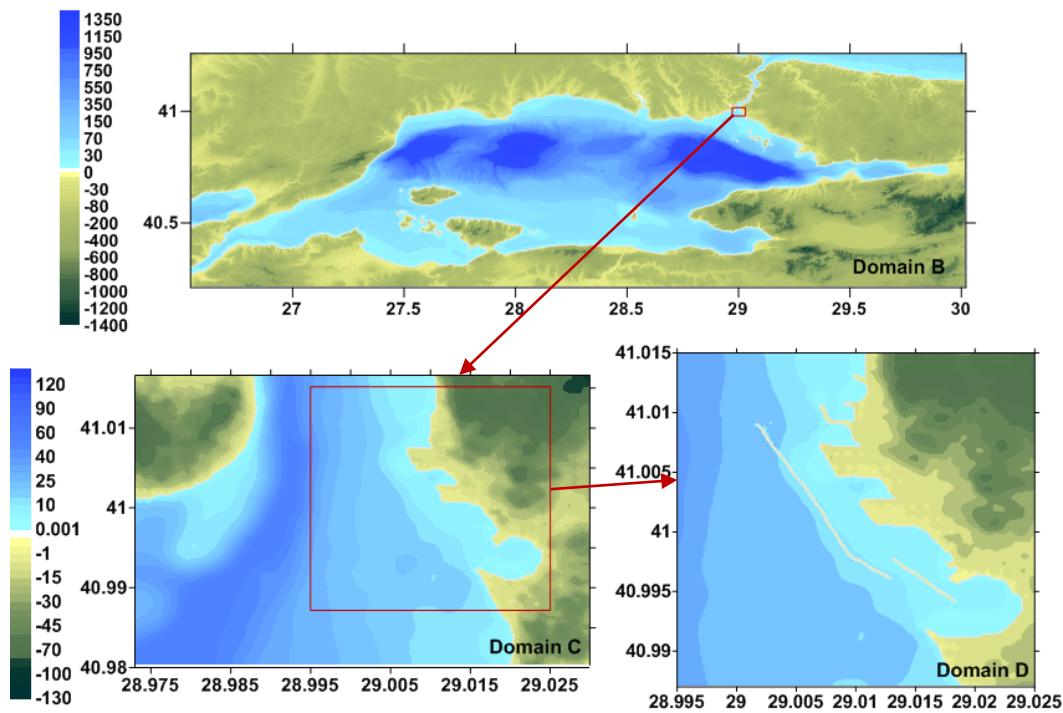
Figure 4.6. Nested study Domains B, C and D used in the simulation of Model 1

Table 4.2. Study domains of Model 1

Domain Name	Grid Size (m)	Coordinates of the Domains
B	90	40.21° – 41.26° N 26.542° – 30.02° E
C	30	40.98° – 41.0165° N 28.973° – 29.030° E
D	10	40.987° – 41.015° N 28.995° – 29.025° E

4.4.2. Bathymetric and Topographic Map of Model 2

Bathymetric and topographic maps of Model 2 are created by using all available data that is purchased DEM and shape data from IMM, GEBCO and some available bathymetric data. The tsunami analysis of the second model is performed by using same nested study domain sizes and coordinates given for Model 1 in Table 4.2. Since this data set includes more detail, obtained maps are more realistic when it is compared with maps of Model 1. General view of the domains of Model 2 are shown in Figure 4.7.
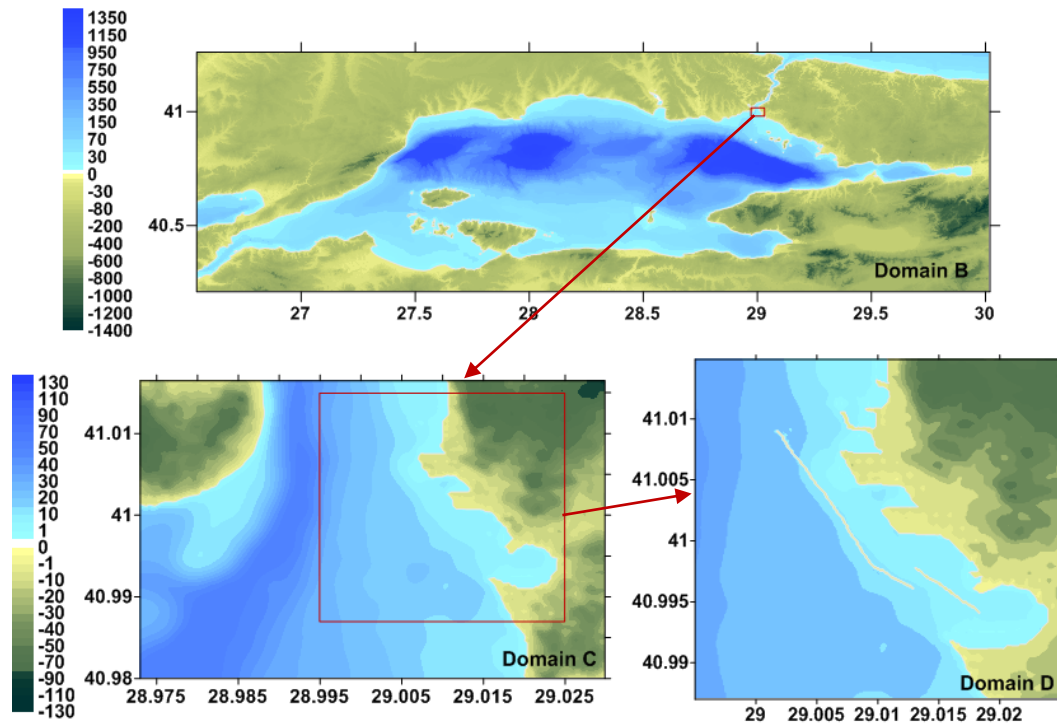
Figure 4.7. Nested study Domains B, C and D used in the simulation of Model 2

4.4.3. Bathymetric and Topographic Map of Model 3

Bathymetric and topographic maps of Model 3 are created by using both purchased DEM and shape data from IMM, GEBCO and some available bathymetric data. Also additional digitization for corrections on coastal line of the region has been performed. The domain sizes and coordinates of Model 3 is given in Table 4.3 and determined nested domains of this model are presented in Figure 4.8.

Table 4.3. Study domains of Model 3

Domain Name	Grid Size (m)	Coordinates of the Domains
B	81	40.5235° – 41.084° N 28.7003° – 29.5564° E
C	27	40.9753° – 41.0197° N 28.9732° – 29.036° E
D	9	40.9834° – 41.0175° N 28.9913° – 29.0286° E
E	3	40.987° – 41.015° N 28.995° – 29.025° E
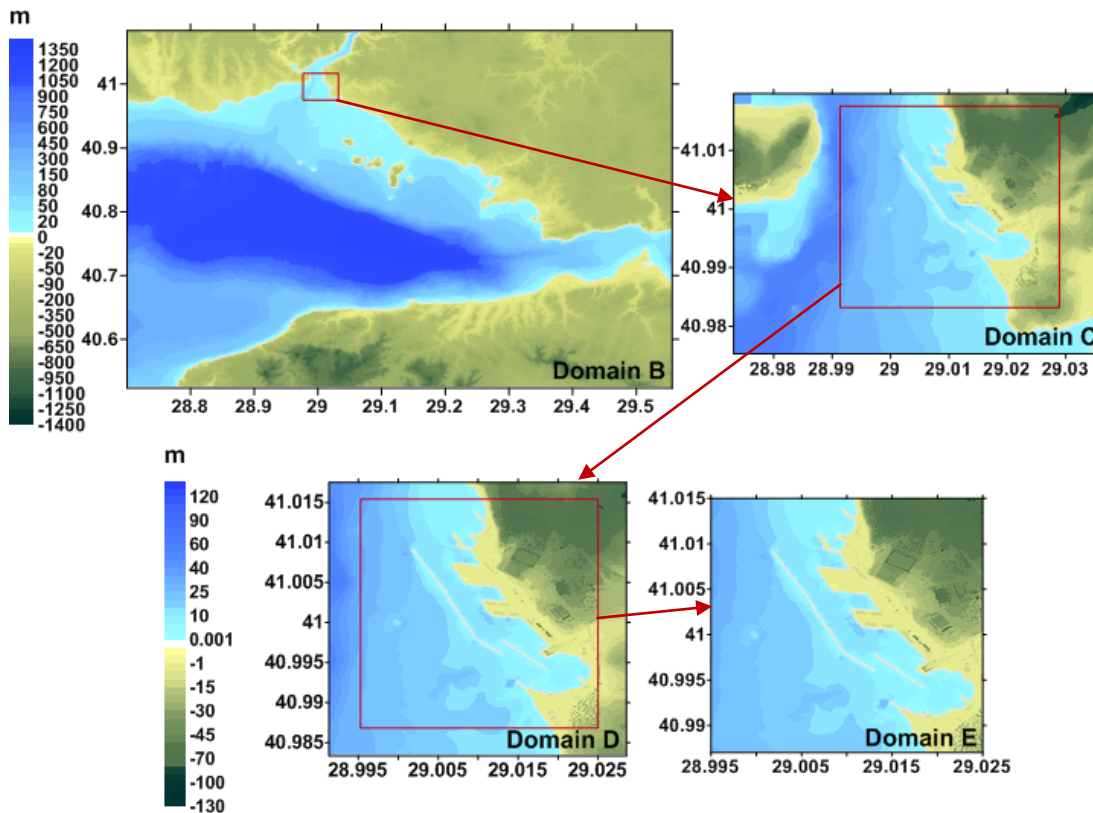
Figure 4.8. Nested study Domains C and D used in the simulation of Model 3

4.4.3. Bathymetric and Topographic Map of Model 4

Bathymetric and topographic maps of Model 4 are created by using purchased DEM data from IMM, GEBCO and some available bathymetric data. Also like in previous models, additional digitization for corrections on coastal line of the region has been performed.

Table 4.4. Study domains of Model 4

Domain Name	Grid Size (m)	Coordinates of the Domains
C	3	40.98° – 41.0165° N 28.973° – 29.030° E
D	1	40.987° – 41.015° N 28.995° – 29.025° E
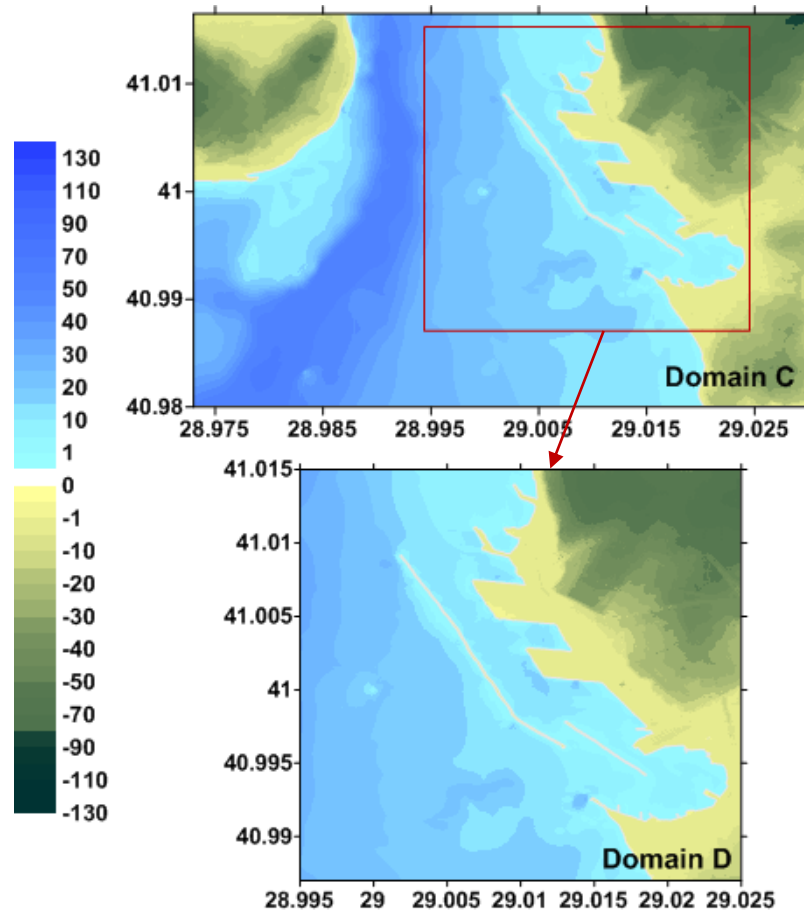
Figure 4.9. Nested study Domains C and D used in the simulation of Model 4

The tsunami analysis of this fourth model is performed by using nested study domains C and D that are constituted with 3 m and 1 m grid size, respectively and given details in Table 4.4. However, Domain B is disused since it covers large area and it is not operable to decrease grid size to 9 m as it is needed to follow one-third grid size rule for NAMI DANCE. In the meantime, decreasing grid size to a very small value results in very large size of matrix, which causes retardation or even slowdown of NAMI DANCE operations. The general view of the mentioned nested study domains for Model 4 are given in Figure 4.9.

4.4.4. Bathymetric and Topographic Map of Model 5

Bathymetric and topographic maps of Model 5 are created by using both purchased DEM and shape data from IMM, GEBCO and some available bathymetric data. Also

like in previous models, additional digitization for corrections on coastal line of the region has been performed.

The tsunami analysis of the fifth model is performed by using same nested study domain sizes and coordinates given for Model 5 in Table 4.4. On the other hand, highest accuracy has been achieved in this final model with the additions of structures' elevations in area of study. In Figure 4.10, the study domains C and D for Model 5 is shown.
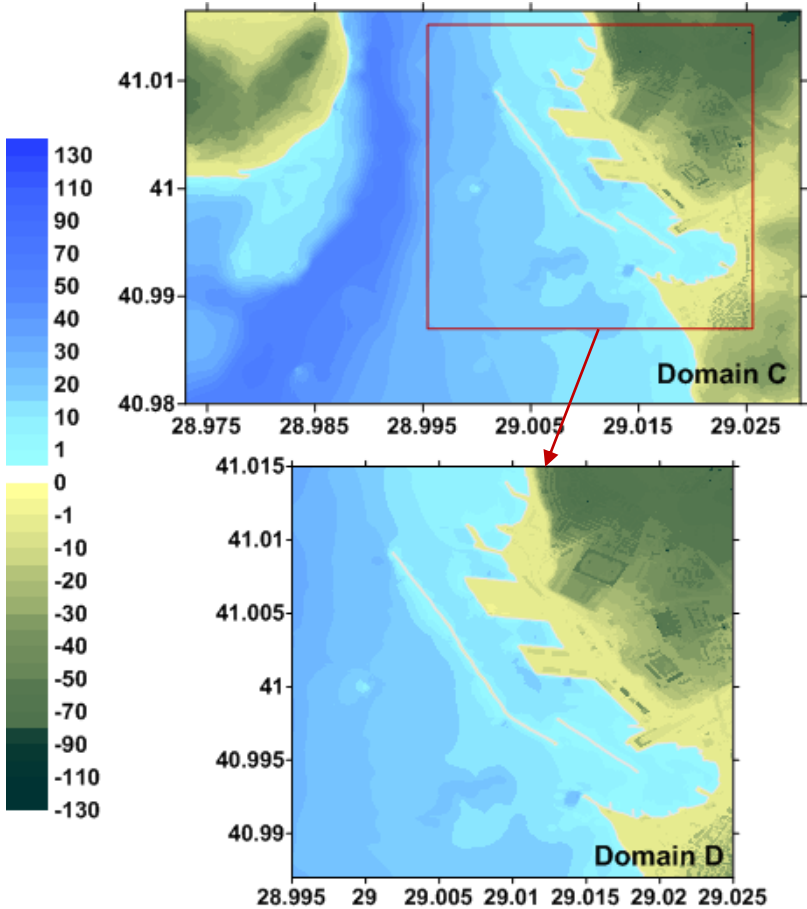
Figure 4.10. Nested study Domains C and D used in the simulation of Model 5

The differences in high resolution maps of Model 4 and Model 5 are more noticeable in Figure 4.11 where the maps are drawn in Global Mapper. In Domain D of Model 5, it is possible to identify each building including the ones with very small dimensions. Even Model 4 includes some information related to existing structures in the area, distortion allowance is high as being the result of interpolation performed to create

DEM. However, the structures are placed in their real dimensions in Model 5 to minimize distortion caused by interpolation. Hereby, Model 5 is specifically prepared to see the change in tsunami inundation by considering the resistance of human-made structures mainly buildings under impact of tsunami waves.

Figure 4.11. Detailed comparison of Domain D for Model 4 and Model 5

4.4.5. Summary of Selected Models

The summary table of models related to data sources, data and model resolutions, selected study domains and type of sources that will be used for each model is given in Table 4.5.

Table 4.5. Summary table of selected models

Model Name	Data Used	Topographic Data Resolution	Smallest Model Resolution	Used Study Domains	Input Source
Model 1	ASTER, GEBCO	30 m	10 m	B, C, D	Rupture
Model 2	All data from IMM	1 m, 5 m	10 m	B, C, D	Rupture
Model 3	All data from IMM	1 m, 5 m	3 m	B, C, D, E	Rupture
Model 4	DEMs from IMM	5 m	1 m	C, D	Border
Model 5	All data from IMM	1 m, 5 m	1 m	C, D	Border

4.5. Selected Gauge Points

At shallower water depths, since waves are sensing the sea bottom, its effects rises tsunami waves significantly. For this reason, numerical gauge points are placed previously defined spatial locations to observe water level fluctuations during the simulation time in the sea and to see the inundation distance and flow depth on land. The full list of chosen gauge points in smallest domain for all models, their depths and coordinates and related figure are in Appendix A. The general view of selected gauge points among all to be used in interpretation of obtained results is given in Figure 4.12.
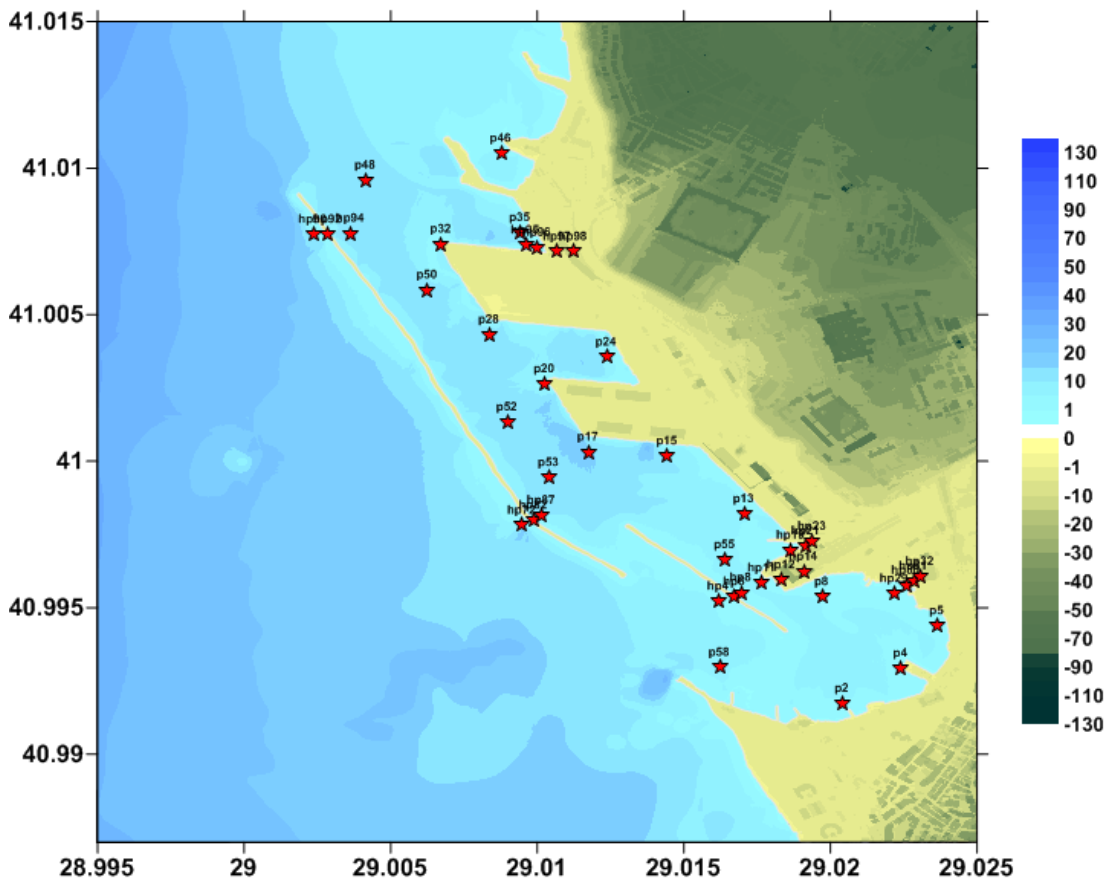
Figure 4.12. The general view of selected numerical gauge points

CHAPTER 5

COMPARISON OF POSSIBLE TSUNAMI SOURCES

Determination of probable tsunami sources in relation to seismic and non-seismic mechanisms becomes significant in case of tsunami analysis. Therefore, in this section, the historical tsunamis and tsunami prone areas in the Sea of Marmara are described. Among these mechanisms, the most effective ones for Haydarpasa Port are selected and compared. The selected sources with their parameters, simulations and results are summarized in the following sections. Besides, procedure in related to applying the selected mechanism as a source in NAMI DANCE program is clarified.

5.1. Historical Earthquakes and Tsunamis in the Sea of Marmara

To perform a reliable tsunami modeling analysis, it is important understand the tectonic characteristics and tsunami risk of the Marmara Sea Basin. Historical tectonic and tsunami records, earthquake and tsunami catalogues are reviewed for this purpose.
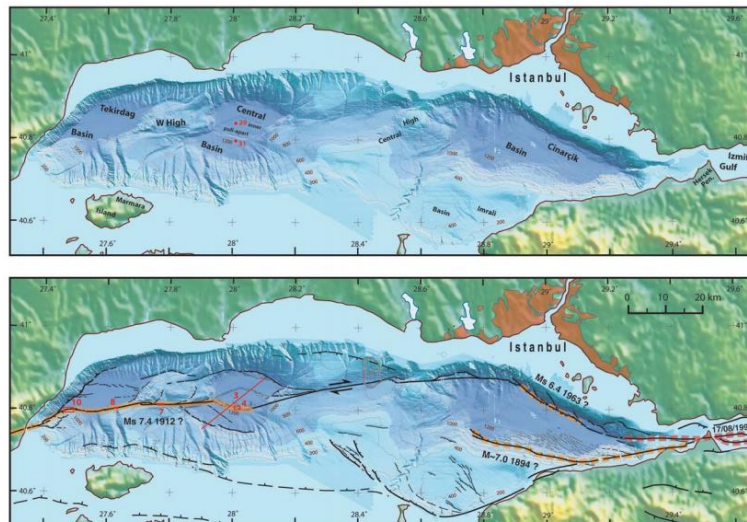
Figure 5.1. Fault zones in the Sea of Marmara (Armijo et. al., 2005 and OYO-IMM, 2007)

Throughout the history, Turkey is highly prone to earthquakes due to availability of many active fault zones in the region. These zones are the North Anatolian Fault Zone (NAFZ) in the North, the East Anatolian Fault Zone (EAFZ) in the East, the Hellenic Arc, the Aegean-Cyprean Arc in the southern Aegean Sea and the Dead Sea Fault Zone (DSFZ).

The Sea of Marmara is located on the western elongation of the North Anatolian Fault Zone. It has three branches, which of two continue in the Sea of Marmara. The faults zones in the region are given in Figure 5.1. NAFZ is one of the important active faults with strike-slip characteristics, which are not likely to generate tsunami. However, according to studies on the past tsunami records, Marmara coasts have been hit by various tsunamis for a long time. Submarine earthquake faults with normal characteristics or submarine landslides might have generated those tsunamis.

Several tsunami catalogues have been prepared for the Sea of Marmara. Based on the latest tsunami catalogue on tsunamis affected around Turkish coasts, which is prepared by Altinok et. al. (2011), the list of significant historical tsunamis in the Sea of Marmara is summarized in Table 5.1. In the list, reliability of the events is also given with respect to GITEC Catalogue criteria. Locations of historical tsunamis in the list are shown in Figure 5.2 if location information is available. According to the list prepared by using the last tsunami catalogue, 35 tsunamis have occurred in the Marmara region. Even, Marmara Sea is a small closed sea with shallow bathymetrical depth and shallow active faults; it is still possible to say that tsunami rates are high in the region.
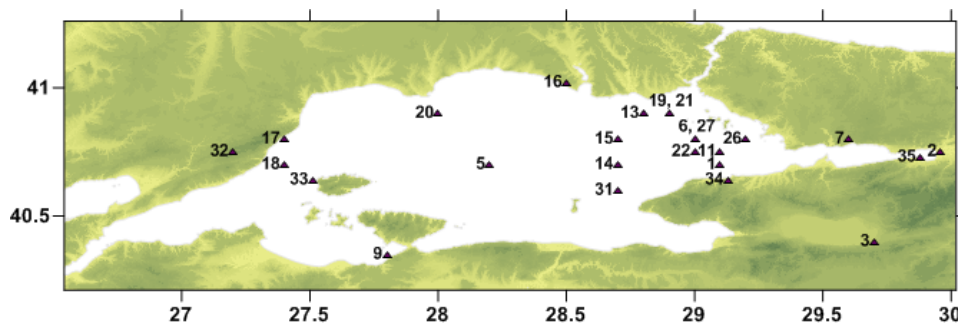
Figure 5.2. Location of historical tsunamis (the ones with estimation of source coordinate information) occurred in the Sea of Marmara from 17th century BC to the recent 1999 event (modified from Altinok et al., 2011)

38

Table 5.1. List of the tsunamigenic event sources in the Sea of Marmara with dates, locations, earthquake magnitudes, tsunami intensities and reliabilities of the events (modified from Altinok et al., 2011)

Number	Year	Source Coordinates	Earthquake Magnitude	Tsunami Intensities: TI1 (Sieberg-Ambraseys Scale)	Reliability* (0-4)
1	123	40.7N 29.1E	7.2	2	3
2	358	40.75N 29.96E	7.4	-	4
3	368	40.4N 29.7E	6.4	-	1 - 2
4	407	-	6.6	3-4	2
5	447	40.7N 28.2E	7.2	4	4
6	478	40.8N 29E	7.3	-	4
7	488	40.8N 29.6E	-	-	1
8	542	-	6.8-6.5	4	1
9	543	40.35N 27.8E	6.6	4	3
10	549	-	-	-	2 - 3
11	553	40.75N 29.1E	7.0	-	4
12	555	-	-	-	1
13	557	40.9N 28.8E	7.0	4	4
14	740	40.7N 28.7E	7.1	3	4
15	989	40.8N 28.7E	7.2	-	4
16	1039	41.02N 28.5E	-	4	1
17	1064	40.8N 27.4E	7.4	-	1
18	1265	40.7N 27.4E	6.6	-	4
19	1332	40.9N 28.9E	6.8	3	3
20	1343	40.9N 28E	7.0	4	4
21	1419	40.9N 28.9E	6.6	-	2
22	1509	40.75N 29E	7.2	3	4
23	1577	-	-	-	1
24	1648	-	6.4	3	4
25	1751	-	-	-	1 - 2
26	1754	40.8N 29.2E	6.8	-	2 - 3
27	1766	40.8N 29E	7.1	2	4
28	1829	-	7.3	2	1
29	1857	-	-	-	1
30	1878	40.7N 30.2E	5.9	3	4
31	1894	40.6N 28.7E	7.3	3	4
32	1912	40.75N 27.2E	7.3	3-4	4
33	1935	40.64N 27.51E	6.4	2-3	4
34	1963	40.64N 29.13E	6.3	-	4
35	1999	40.73N 29.88E	7.4	3	4

* Reliability of the events according to GITEC Catalogue criteria (0: very improbable, 1: improbable, 2: questionable, 3: probable and 4: definite tsunami)

In OYO-IMM Report (2007), it is indicated that maximum tsunami run-up height (6 m) observed after 1509 Earthquake in Istanbul, which is followed by 1894 Earthquake with 4-4.5 m run-up height with respect to historical documents.

It is clearly seen that the characteristics of possible tsunami sources have already been obtained for the region in previous studies. However, a complete tsunami inundation analysis using recent data processing and computational techniques will provide better analysis to understand the effects of different levels of tsunamis on a specific critical structure located in Marmara coasts (Aytore, Yalciner et al., 2013).

5.2. Selected Seismic Sources and Related Rupture Parameters in the Sea of Marmara

OYO-IMM Report (2007) has been examined in detail and critical active sources are determined for Marmara region by Ayca (2012). As the author stated, the critical active faults for the Sea of Marmara are Prince's Islands Strike Slip (PI) Fault, Prince's Islands Normal (PIN) Fault, Ganos Strike Slip (GA) Fault, Yalova Normal (YAN) Fault, Central Marmara Normal (CMN) Fault, and the combination of Prince's Islands and Ganos Strike Slip (PI+GA) Faults. According to presented results by Ayca, it is revealed that the tsunami generated by the sources YAN, PIN and CMN cause higher water level, flow depth and stronger current velocities near Haydarpasa Port. Thus, these segmented faults are selected to compare by performing new simulations for Haydarpasa Port and find out the most critical one to use in simulations as a final source and create source to be used in high resolution maps since different procedure has to be followed for them, which will be explained in the next section.

The rupture parameters of each segment for selected faults YAN, PIN and CMN are given in Table 5.2. By considering uncertainties, the vertical displacements are selected as 5 m like in Ayca's study instead of considering OYO-IMM report in which vertical displacements were selected as around 2 to 3 m for normal segments. Ayca explained this vertical displacement change by giving 2011 Great East Japan tsunami example where vertical displacement was almost two times more than expected.

Maps of Model 2 are used in the source determination analyses. This is because, all available data is used for creation of maps of this model. It is expected to obtain more

accurate results in comparison with Model 1. Besides, there is no need to follow a different procedure related to source since maps are not in high resolution and 10 m resolution is sufficient to have a general idea on the most effective source for selected region. The process time is more adequate than high resolution models.

Table 5.2. Estimated rupture parameters for each segment of each source YAN, PIN and CMN

	Lon. (°)	Lat. (°)	Depth (m)	Strike (°)	Dip (°)	Rake (°)	Length (m)	Width (m)	Vertical Disp. (m)
	29.47103	40.72115	1978	257.96	70	195	7058	17027	5
	29.38946	40.70850	1960	261.14	70	195	6873	17027	5
	29.30920	40.69851	1823	260.98	70	195	10952	17027	5
	29.18143	40.68121	1681	262.35	70	270	4448	17027	5
YAN	29.12936	40.67650	1557	273.96	70	270	4562	17027	5
	29.07651	40.67891	1252	283.78	70	270	10021	17027	5
	28.96007	40.69843	1219	294.84	70	270	3154	17027	5
	28.96202	40.71005	1178	284.90	70	270	14043	17027	5
	29.12942	40.75691	744	108.15	70	270	8753	17027	5
	29.06928	40.78610	740	123.15	70	270	6024	17027	5
PIN	28.99465	40.81653	779	118.85	70	270	7148	17027	5
	28.90432	40.87251	1210	129.90	70	270	9834	17027	5
	28.19394	40.6126	1924	276.59	70	270	9505	17027	5
	28.08215	40.6206	1922	279.18	70	270	7069	17027	5
CMN	27.99943	40.6294	1917	299.07	70	270	10705	17027	5
	27.88744	40.6742	1598	283.92	70	270	7850	17027	5
	27.79683	40.6895	1637	291.38	70	270	7269	17027	5

5.2.1. Yalova Normal (YAN) Fault Simulation

YAN simulation is performed by using NAMI DANCE in nested domains by considering rupture parameters given previous section. The simulation time is selected as 90 minutes depending on the location of tsunami source with respect to the Haydarpasa Port.

The initial sea state, arrival time of maximum wave in Domain B and distributions of maximum water elevation in Domain B and near shoreline of Haydarpasa Port (in Domain C) after breaking of YAN fault are given in Figure 5.3.

(a)   **(b)**

(c)
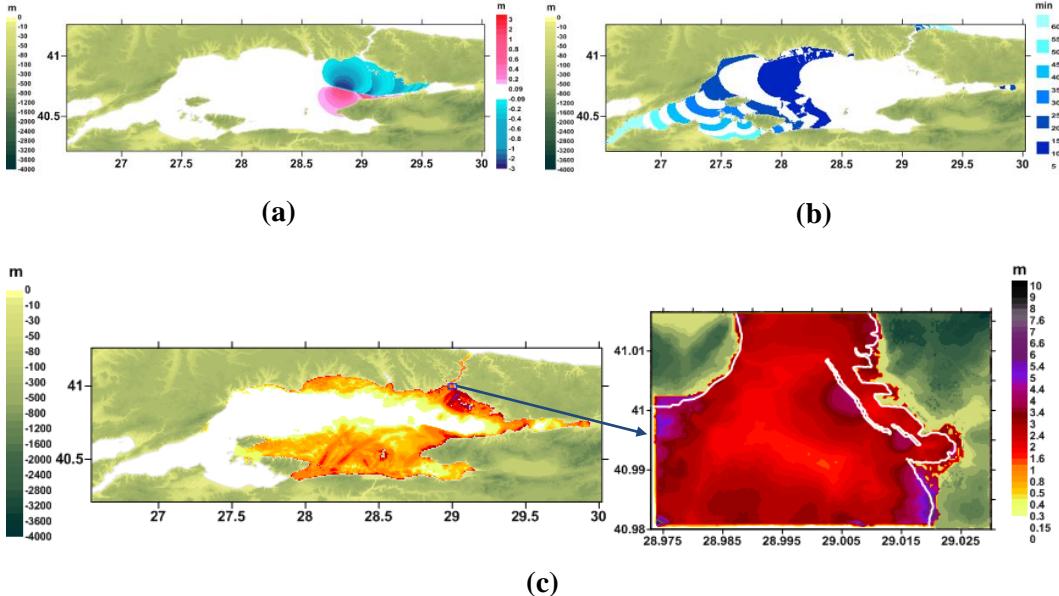
Figure 5.3. (a) Initial sea state in Domain B, (b) distribution of arrival time of first wave in Domain B, (c) distribution of maximum water surface elevation in Domain B and Domain C after YAN simulations

5.2.2. Prince's Islands Normal (PIN) Fault Simulation

PIN simulation is performed by using NAMI DANCE in nested domains with duration of 90 minutes like YAN simulation.

The initial sea state, arrival time of maximum wave in Domain B and distributions of maximum water elevation in Domain B and near shoreline of Haydarpasa Port (in Domain C) after breaking of PIN fault are given in Figure 5.4.
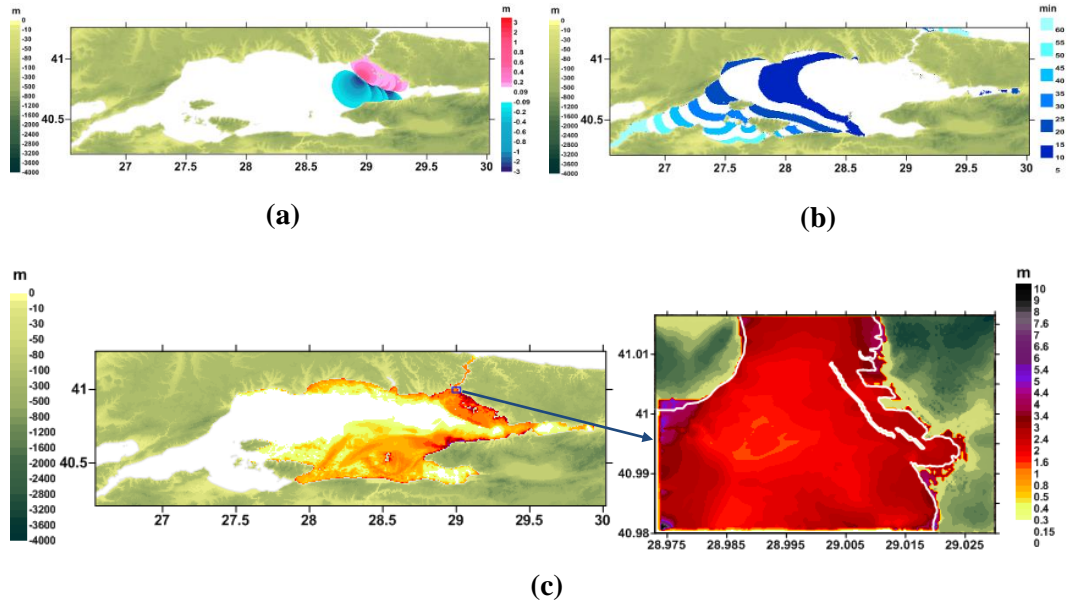
Figure 5.4. (a) Initial sea state in Domain B, (b) distribution of arrival time of first wave in Domain B, (c) distribution of maximum water surface elevation in Domain B and Domain C after PIN simulations

5.2.3. Central Marmara Normal (CMN) Fault Simulation

CMN simulation is performed by using NAMI DANCE in nested domains with duration of 90 minutes like YAN and PIN simulations.

The initial sea state, arrival time of maximum wave in Domain B and distributions of maximum water elevation in Domain B and near shoreline of Haydarpasa Port (in Domain C) after breaking of CMN fault are given in Figure 5.5.

43
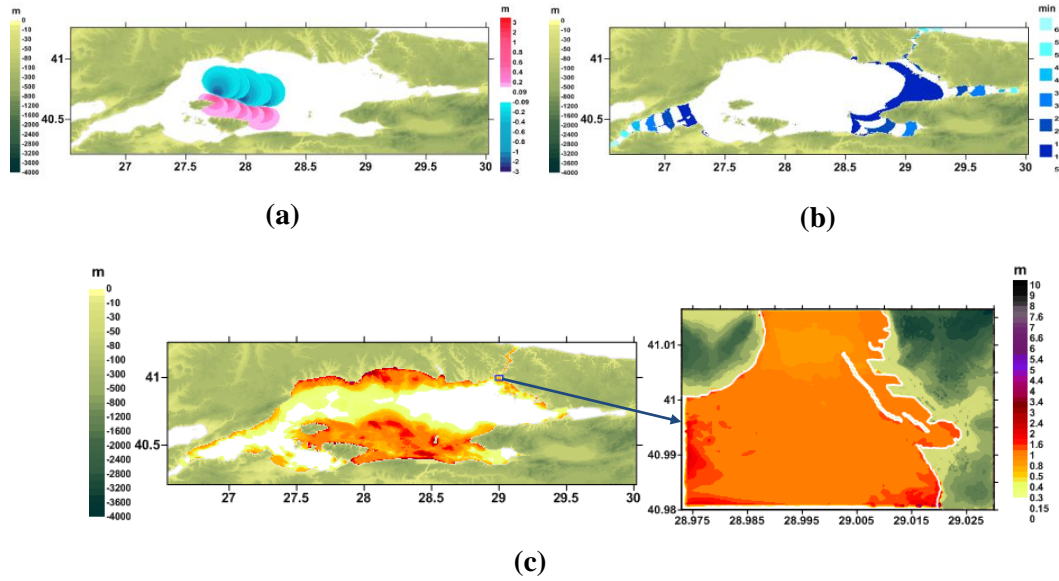
Figure 5.5. (a) Initial sea state in Domain B, (b) distribution of arrival time of first wave in Domain B, (c) distribution of maximum water surface elevation in Domain B and Domain C after CMN simulations

5.3. Source Determination for Tsunami Analyses and Its Implementation in NAMI DANCE for High Resolution Simulations

For Model 4 and Model 5, instead of using available earthquake rupture parameters of (rupture source input) like in all other models, time series of water surface fluctuation inputted arbitrarily from the border of largest domain (border source input) are used to create initial tsunami wave motion. In these two models, border source preferred to be used since all selected sources are in the Sea of Marmara and outside of selected Domain C, which is the largest domain for these two high resolution simulations. The aim of this procedure change is reduce duration of simulation to a feasible level.

The critical source for the region will be determined according to obtained results. However, it is important to primarily indicate border source to be used in Model 4 and Model 5 simulations.

Time series of water surface fluctuation to be used as border source are obtained from performed nested domain simulations of YAN, PIN and CMN in pervious section. Due to determine border source for Model 4 and Model 5, some gauges placed on the border

of Domain C. The gauges placed on the border of Domain C are given in Figure 5.6 and maximum positive and negative water levels obtained end of each simulation are tabulated in Table 5.3.
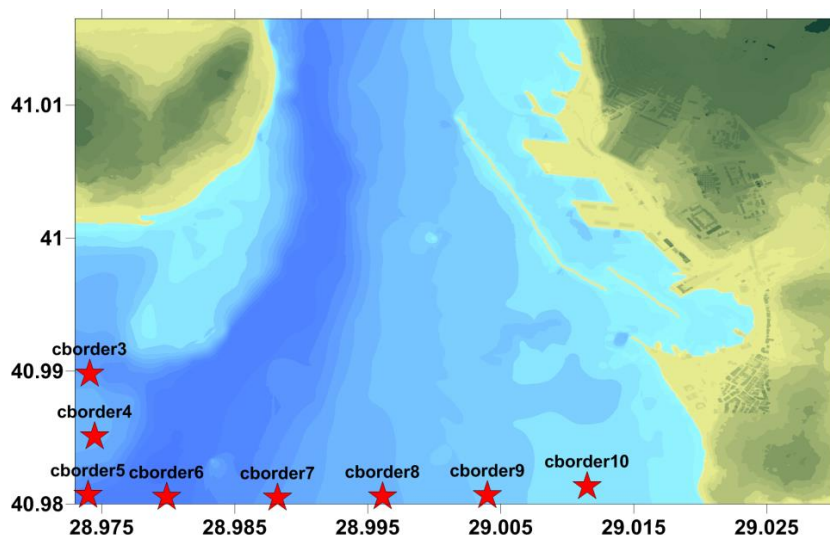
Figure 5.6. The border gauges placed in Domain C to determine the border source

Table 5.3. Maximum positive and negative wave amplitudes observed at each border gauge as result of YAN, PIN and CMN sources

Border gauge	Depth	YAN		PIN		CMN	
		Max. (+)ve amp. (m)	Max. (-)ve amp. (m)	Max. (+)ve amp. (m)	Max. (-)ve amp. (m)	Max. (+)ve amp. (m)	Max. (-)ve amp. (m)
cborder3	8.4	3.4	-3.2	3.1	-2.5	1.9	-0.9
cborder4	20.0	2.9	-2.9	2.8	-2.2	1.5	-0.8
cborder5	20.0	5.2	-2.8	5.6	-2.5	1.8	-0.7
cborder6	15.3	2.3	-2.2	2.7	-2.5	1.7	-0.8
cborder7	21.7	3.2	-1.8	1.8	-2.2	1.4	-0.6
cborder8	26.3	3.0	-1.8	2.3	-2.2	1.1	-0.6
cborder9	16.5	3.2	-1.9	2.9	-2.1	1.2	-0.7
cborder10	8.9	2.6	-3.2	2.0	-2.5	1.5	-0.8

According to maximum water distributions in Domain C drawn in Section 5.2, it is clearly seen that CMN is not a critical fault for Haydarpasa Port if it is compared with YAN and PIN cases since maximum wave amplitudes are around 1-2 m where YAN and PIN results are around 2-4 m. In maximum positive and negative wave amplitudes

45

at the border gauges tabulated below, it is also possible to identify the smaller wave amplitudes created by CMN source. Therefore, CMN fault will not be considered as a critical source henceforth in this study.

On the other hand, it is hard to determine from the table whether YAN or PIN is the critical fault for the region and which one should be used as a source in the series of tsunami analysis to be performed in NAMI DANCE. The comparison of water level fluctuation at some of previously determined border gauges after YAN and PIN simulations, which are given in Figure 5.7, are prepared to decide on the final source to be used in the study from now on.
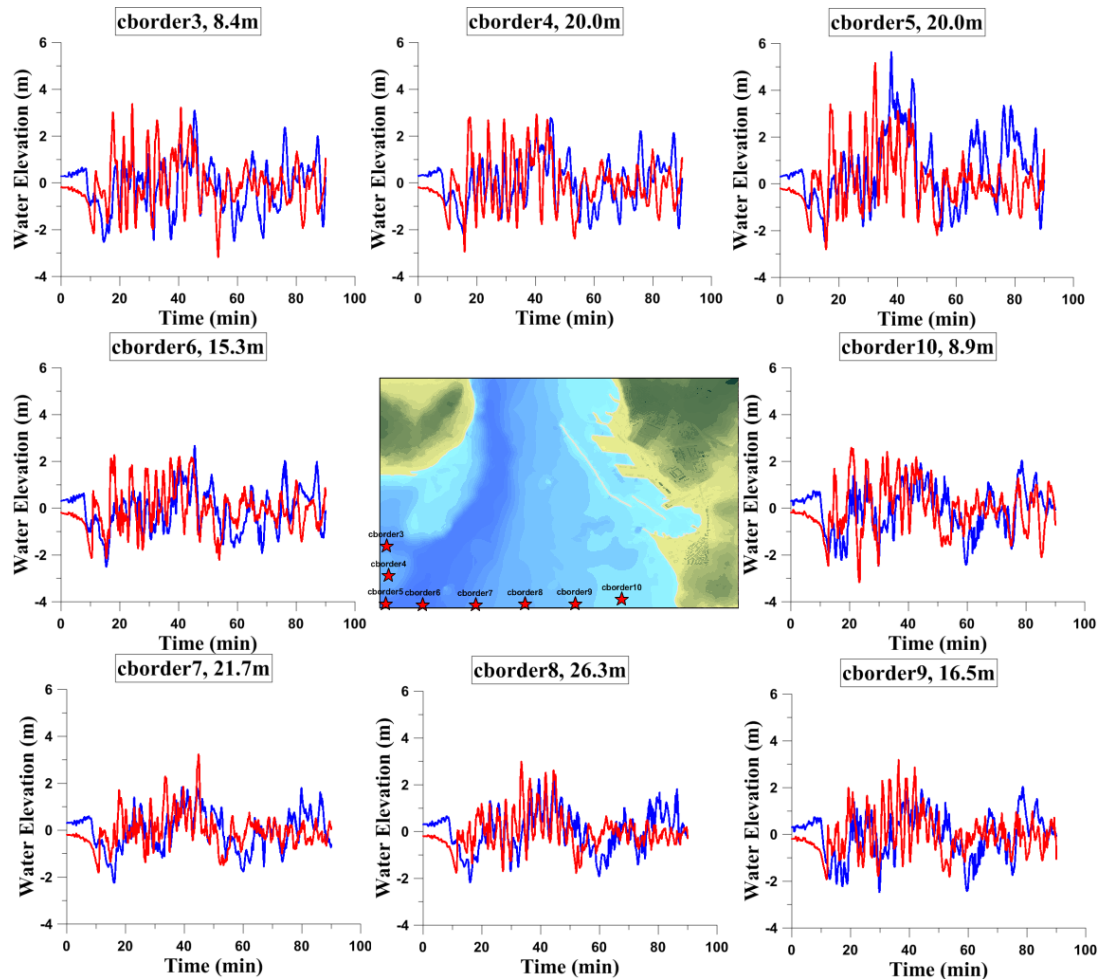
Figure 5.7. Comparison of water level fluctuations at border gauges obtained after YAN and PIN simulations (In the figure, red lines represent YAN simualtion results and blue lines represent PIN simualtion results)

When all graphs are carefully examined, it is determined that even the graphs of PIN and YAN faults are quite close to each other, YAN fault is more effective in the study region. Hereby, source YAN used in the simulations of Model 1, Model 2 and Model 3 from this moment during the study.

On the other hand, YAN fault's graphs should be analyzed more to select a border gauge, of which water level fluctuations will be used as border source in Model 4 and Model 5. When locations of all gauges given in the Figure 5.6 are considered, "cborder3" and "cborder4" are located far from the port area and right across to the breakwaters, which will block tsunami waves and cause less fluctuation inside the port. "cborder5" is located on the corner of the selected domain where instabilities may occur causing decrease in reliability of the data compared to other gauges as well. Hereby, the selection is carried out between the gauges at "cborder6", "cborder7", "cborder8" "cborder9", and "cborder10". According to graphs, it is identified that "cborder9", which shows higher water level changes, is more effective in Domain C. Thereof, "cborder9" results obtained from YAN simulations are selected to be used as border source in two high resolution simulations, Model 4 and Model 5.
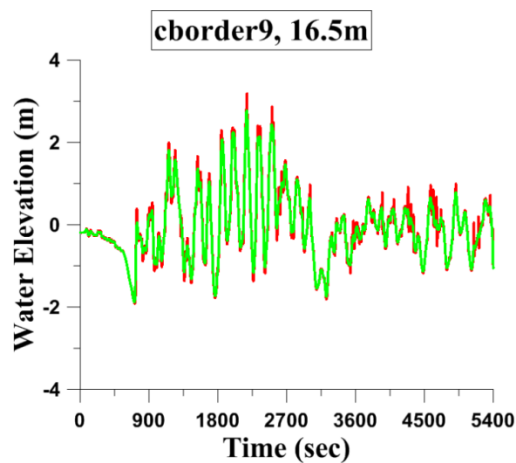
Figure 5.8. Before and after smoothing of water level fluctuation graph at "cborder9" obtained from YAN simulation shown by red and green lines, respectively

In case of high resolution models, after selection of border gauge to implement NAMI DANCE as a source, the chosen water fluctuation file saved with data extension that covers water elevations at "cborder9" on each predetermined time step until the end of

the simulation, which is 90 minutes in this case. Next, time column changed to seconds by multiplying it with 60 and a code is written in Visual Studio Intel Fortran for compatibility of the time steps since time step used in B, C, D nested simulations was 0.05 seconds and time step will be used in C, D nested high resolution simulations is 0.02 seconds. The written code interpolates required missing values for compatibility. In addition, smoothing of water level fluctuation graph is carried out by again written code in Visual Studio Intel Fortran. This is because to make the graph more compatible with general wave motion. The time histories of water surface fluctuations inputted at the border is shown in Figure 5.8. In the figure, the computed and smoothed time histories are shown together.

CHAPTER 6

TSUNAMI HAZARD ANALYSIS FOR HAYDARPASA PORT

The results of performed tsunami simulations presented in this section. According to results, maps related to distribution of maximum positive wave amplitudes and bar charts represent the run-up heights (maximum near shore positive tsunami amplitudes) during the entire simulation time, in Domain D are drawn for each model. The distribution of minimum water elevations (negative wave amplitudes) and maximum flow depths on land (inundation maps) are also presented for each model in this section. In addition to these, maximum and minimum water surface elevations and arrival time of maximum and minimum waves at each gauge points are also tabulated.

The duration of simulations performed in NAMI DANCE is 90 minutes for all models to understand the coastal amplifications of tsunami at selected locations. Since largest tsunami waves hits the area in first 45 minutes, 90 minutes duration is convenient to obtain reliable results include wave reflections. The duration also covers the arrival of wave reflected from southern coast of the Marmara Sea. The selected time step is 0.05 seconds for Model 1 and 2, 0.0125 seconds for Model 3 and 0.02 seconds for Model 3 and Model 4 and 0.005 for Model 5. Friction coefficient for each model is taken as zero.

6.1. Tsunami Analysis for Model 1

The tsunami parameters of Model 1 are computed near shorelines in Domain D by NAMI DANCE. The selected computed results are drawn in Table 6.1 and arrival time of initial and maximum tsunami waves and maximum positive and negative wave amplitudes at selected gauges are tabulated in Table 6.2.

Table 6.1. Computed tsunami parameters of Model 1
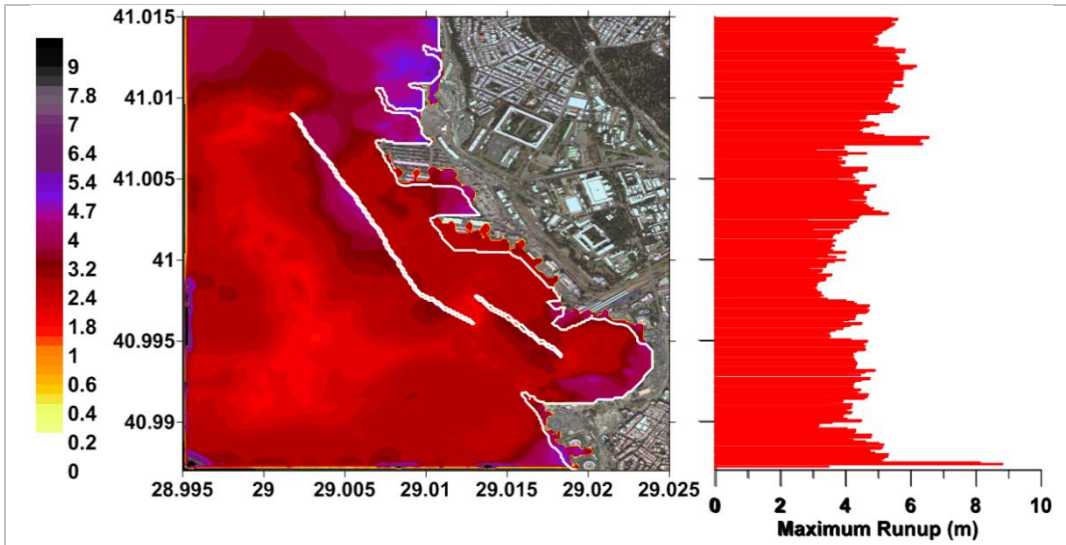
Distribution of maximum (+)ve wave amplitudes on the left and the run-up heights (maximum near shore (+)ve tsunami amplitudes) on the right at land in Domain D during the entire tsunami simulation
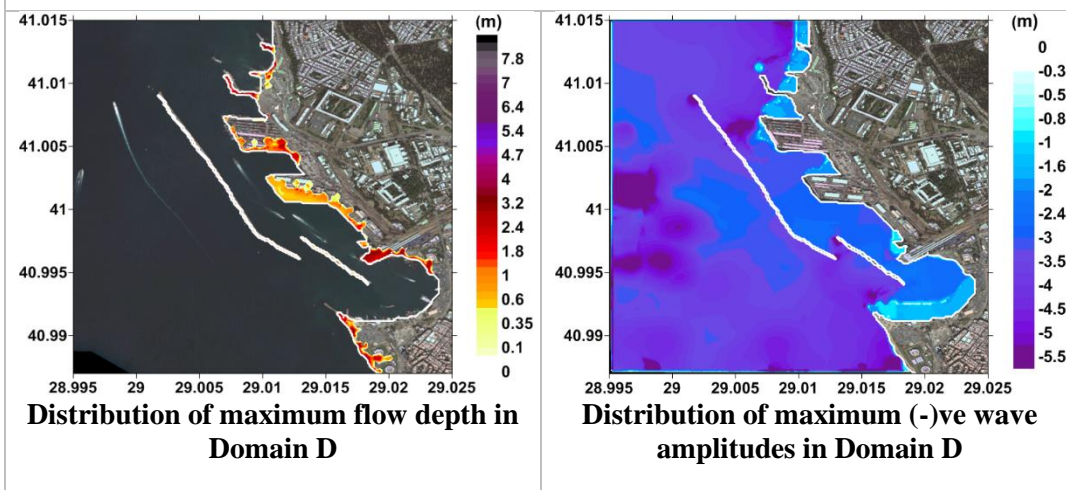
Distribution of maximum flow depth in Domain D

Distribution of maximum (-)ve wave amplitudes in Domain D

The maximum near shore positive tsunami amplitude	: 6.0 m
The minimum near shore negative tsunami amplitude	: -5.0 m
The maximum flow depth	: 4.5 m
Maximum inundation distance	: 170 m

50

Table 6.2. Maximum positive and negative wave amplitudes and arrival time of initial and maximum wave of Model 1 at selected numerical gauge points with their water depths and coordinates

Name of Gauge Pt.	Depth (m)	Longitude (°)	Latitude (°)	Arrival time of initial wave (min)	Arrival time of max.wave (min)	Max. (+)ve amp. (m)	Max. (-)ve amp. (m)
hp4	7.0	29.0162	40.9952	0	36	3.2	-3.4
hp6	-4.0	29.0167	40.9954	0	0	0.0	0.0
hp8	6.0	29.0169	40.9955	0	36	3.2	-2.2
hp11	5.0	29.0177	40.9958	0	37	3.1	-2.7
hp12	-1.0	29.0183	40.9959	16	37	3.4	0.0
hp14	-1.0	29.0191	40.9962	16	37	3.4	0.0
hp19	-5.0	29.0187	40.997	0	0	0.0	0.0
hp21	-6.0	29.0192	40.9971	0	0	0.0	0.0
hp23	-8.0	29.0194	40.9973	0	0	0.0	0.0
hp29	6.0	29.0222	40.9955	0	36	2.8	-2.5
hp30	0.1	29.0226	40.9958	0	36	3.2	-0.1
hp31	-3.0	29.0228	40.9959	36	36	3.6	0.0
hp32	-4.0	29.0231	40.9961	36	36	4.3	0.0
hp72	10.0	29.0095	40.9978	0	34	2.9	-3.5
hp82	-4.0	29.0099	40.998	0	0	0.0	-0.2
hp87	10.0	29.0102	40.9981	0	36	3.0	-2.7
hp90	20.0	29.0024	41.0077	0	34	3.2	-3.9
hp92	10.0	29.0029	41.0077	0	68	4.0	-3.8
hp94	20.0	29.0036	41.0078	0	68	3.9	-4.0
hp95	2.0	29.0096	41.0074	0	62	5.1	-1.9
hp96	2.0	29.01	41.0073	0	62	5.8	-1.9
hp97	-9.0	29.0107	41.0071	0	0	0.0	0.0
hp98	-10.0	29.0112	41.0071	0	0	0.0	0.0
p2	2.0	29.0204	40.9917	0	64	4.1	-1.6
p4	2.0	29.0224	40.9929	0	64	3.7	-1.7
p5	2.0	29.0236	40.9944	0	36	4.2	-1.7

Table 6.2. (Continued)

Name of Gauge Pt.	Depth (m)	Longitude (°)	Latitude (°)	Arrival time of initial wave (min)	Arrival time of max.wave (min)	Max. (+)ve amp. (m)	Max. (-)ve amp. (m)
p8	6.0	29.0197	40.9954	0	36	2.5	-2.3
p13	5.0	29.0171	40.9982	0	36	2.8	-3.0
p15	8.0	29.0144	41.0002	0	36	2.6	-3.0
p17	9.0	29.0117	41.0003	0	36	2.9	-2.9
p20	6.0	29.0103	41.0026	0	21	2.9	-3.0
p24	2.0	29.0124	41.0035	0	63	4.3	-1.9
p28	6.0	29.0084	41.0043	0	63	3.0	-3.1
p32	5.0	29.0067	41.0074	0	68	3.0	-5.0
p35	2.0	29.0094	41.0078	0	67	4.4	-1.8
p46	3.0	29.0088	41.0105	0	67	4.5	-3.0
p48	10.0	29.0041	41.0096	0	68	3.4	-3.6
p50	3.0	29.0063	41.0058	0	21	2.7	-3.0
p52	6.0	29.009	41.0013	0	21	2.6	-3.0
p53	7.0	29.0104	40.9994	0	36	2.9	-2.8
p55	6.0	29.0164	40.9966	0	37	2.8	-2.7
p58	4.0	29.0162	40.993	0	36	2.5	-4.0

6.2. Tsunami Analysis for Model 2

The tsunami parameters of Model 2 are computed near shorelines in Domain D by NAMI DANCE. The selected computed results are drawn in Table 6.3 and arrival time of initial and maximum tsunami waves and maximum positive and negative wave amplitudes at selected gauges are tabulated in Table 6.4.

Table 6.3. Computed tsunami parameters of Model 2

Distribution of maximum (+)ve wave amplitudes on the left and the run-up heights (maximum near shore (+)ve tsunami amplitudes) on the right at land in Domain D during the entire tsunami simulation

Distribution of maximum flow depth in Domain D

Distribution of maximum (-)ve wave amplitudes in Domain D

The maximum near shore positive tsunami amplitude	: 7.0 m
The minimum near shore negative tsunami amplitude	: -5.0 m
The maximum flow depth	: 5.4 m
Maximum inundation distance	: 460 m

Table 6.4. Maximum positive and negative wave amplitudes and arrival time of initial and maximum wave of Model 2 at selected numerical gauge points with their water depths and coordinates

Name of Gauge Pt.	Depth (m)	Longitude (°)	Latitude (°)	Arrival time of initial wave (min)	Arrival time of max.wave (min)	Max. (+)ve amp. (m)	Max. (-)ve amp. (m)
hp4	3.2	29.0162	40.9952	0	32	2.8	-3.2
hp6	1.0	29.0167	40.9954	0	32	3.1	-1.0
hp8	3.4	29.0169	40.9955	0	41	2.1	-2.3
hp11	5.0	29.0177	40.9958	0	41	2.1	-2.7
hp12	-1.2	29.0183	40.9959	17	22	2.2	0.0
hp14	-26.5	29.0191	40.9962	0	0	0.0	0.0
hp19	0.8	29.0187	40.997	0	23	2.6	-0.7
hp21	-3.6	29.0192	40.9971	0	0	0.0	0.0
hp23	-3.2	29.0194	40.9973	0	0	0.0	0.0
hp29	2.1	29.0222	40.9955	0	36	2.5	-2.1
hp30	2.0	29.0226	40.9958	0	36	2.6	-1.2
hp31	-1.3	29.0228	40.9959	17	36	2.6	0.0
hp32	-2.6	29.0231	40.9961	36	36	2.7	0.0
hp72	10.8	29.0095	40.9978	0	35	2.5	-3.7
hp82	-3.0	29.0099	40.998	0	0	0.0	-0.2
hp87	8.9	29.0102	40.9981	0	23	2.6	-2.8
hp90	9.2	29.0024	41.0077	0	35	2.5	-2.6
hp92	1.6	29.0029	41.0077	0	35	2.8	-1.6
hp94	12.2	29.0036	41.0078	0	21	2.3	-3.0
hp95	5.3	29.0096	41.0074	0	29	2.9	-3.8
hp96	0.9	29.01	41.0073	0	29	3.1	-0.9
hp97	-2.7	29.0107	41.0071	21	29	3.1	0.0
hp98	-2.8	29.0112	41.0071	0	0	0.0	0.0
p2	3.8	29.0204	40.9917	0	36	2.2	-1.9
p4	2.0	29.0224	40.9929	0	32	2.3	-1.8
p5	3.5	29.0236	40.9944	0	36	2.6	-2.5

54

Table 6.4. (Continued)

Name of Gauge Pt.	Depth (m)	Longitude (°)	Latitude (°)	Arrival time of initial wave (min)	Arrival time of max.wave (min)	Max. (+)ve amp. (m)	Max. (-)ve amp. (m)
p8	4.8	29.0197	40.9954	0	36	2.1	-2.0
p13	6.4	29.0171	40.9982	0	18	2.2	-3.5
p15	10.2	29.0144	41.0002	0	22	2.6	-3.0
p17	16.1	29.0117	41.0003	0	22	2.6	-2.8
p20	2.3	29.0103	41.0026	0	22	2.1	-2.3
p24	9.4	29.0124	41.0035	0	33	2.6	-3.0
p28	12.4	29.0084	41.0043	0	22	1.9	-2.7
p32	5.0	29.0067	41.0074	0	21	2.3	-2.7
p35	10.7	29.0094	41.0078	0	29	2.7	-3.8
p46	5.2	29.0088	41.0105	0	29	2.9	-2.5
p48	11.6	29.0041	41.0096	0	21	1.9	-2.9
p50	12.0	29.0063	41.0058	0	21	2.0	-3.2
p52	11.6	29.009	41.0013	0	22	2.4	-2.7
p53	11.3	29.0104	40.9994	0	22	2.4	-2.8
p55	5.8	29.0164	40.9966	0	18	2.1	-3.9
p58	6.0	29.0162	40.993	0	32	2.1	-4.6

6.3. Tsunami Analysis for Model 3

The tsunami parameters of Model 3 are computed near shorelines in Domain D by NAMI DANCE. The selected computed results are drawn in Table 6.5 and arrival time of initial and maximum tsunami waves and maximum positive and negative wave amplitudes at selected gauges are tabulated in Table 6.6.

Table 6.5. Computed tsunami parameters of Model 3
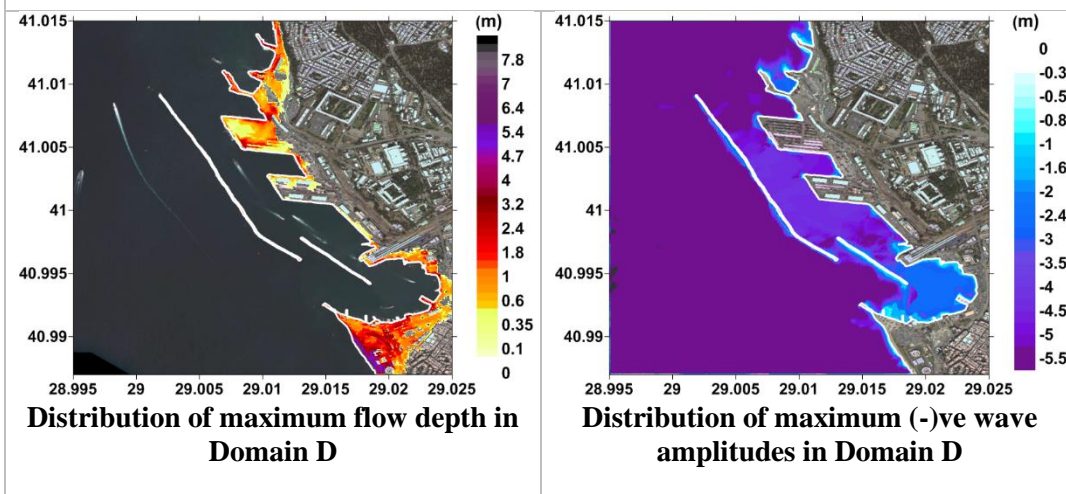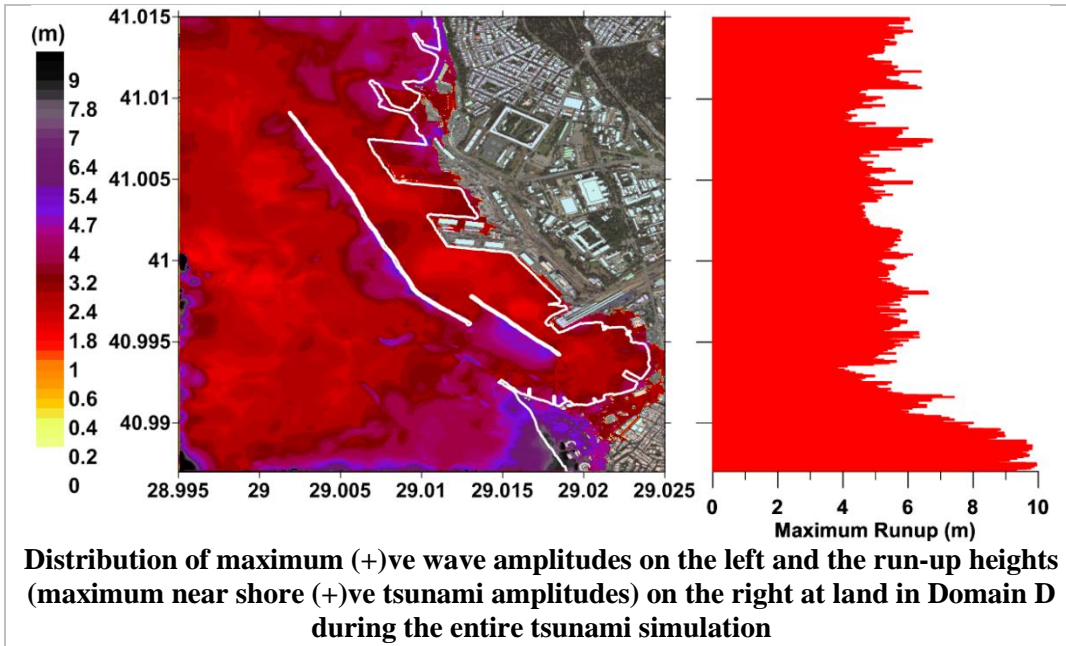
Distribution of maximum (+)ve wave amplitudes on the left and the run-up heights (maximum near shore (+)ve tsunami amplitudes) on the right at land in Domain D during the entire tsunami simulation

Distribution of maximum flow depth in Domain D

Distribution of maximum (-)ve wave amplitudes in Domain D

The maximum near shore positive tsunami amplitude	: 6.5 m
The minimum near shore negative tsunami amplitude	: -6 m
The maximum flow depth	: 5.5 m
Maximum inundation distance	: 460 m

Table 6.6. Maximum positive and negative wave amplitudes and arrival time of initial and maximum wave of Model 3 at selected numerical gauge points with their water depths and coordinates

Name of Gauge Pt.	Depth (m)	Longitude (°)	Latitude (°)	Arrival time of initial wave (min)	Arrival time of max.wave (min)	Max. (+)ve amp. (m)	Max. (-)ve amp. (m)
hp4	2.7	29.0162	40.9952	3	45	4.6	-2.7
hp6	-2.0	29.0167	40.9954	18	45	5.4	0.0
hp8	3.5	29.0169	40.9955	3	46	2.6	-2.9
hp11	4.1	29.0177	40.9958	3	45	2.5	-3.5
hp12	-2.3	29.0183	40.9959	21	46	3.0	0.0
hp14	-9.4	29.0191	40.9962	0	0	0.0	0.0
hp19	2.7	29.0187	40.997	4	22	3.5	-1.3
hp21	-5.2	29.0192	40.9971	0	0	0.0	0.0
hp23	-3.2	29.0194	40.9973	0	0	0.0	0.0
hp29	2.3	29.0222	40.9955	4	45	3.1	-2.3
hp30	2.0	29.0226	40.9958	4	45	3.6	-1.5
hp31	-2.2	29.0228	40.9959	19	45	3.2	0.0
hp32	-10.8	29.0231	40.9961	0	0	0.0	0.0
hp72	9.4	29.0095	40.9978	3	35	4.4	-7.2
hp82	-4.0	29.0099	40.998	32	35	5.6	0.0
hp87	9.5	29.0102	40.9981	3	34	2.8	-4.2
hp90	8.6	29.0024	41.0077	3	32	3.7	-5.7
hp92	-2.0	29.0029	41.0077	15	32	4.7	0.0
hp94	12.5	29.0036	41.0078	3	21	2.6	-5.0
hp95	3.8	29.0096	41.0074	3	34	4.2	-3.8
hp96	0.9	29.01	41.0073	4	34	5.1	-0.8
hp97	-2.7	29.0107	41.0071	17	34	5.5	0.0
hp98	-11.3	29.0112	41.0071	0	0	0.0	0.0
p2	4.0	29.0204	40.9917	3	45	3.3	-2.9
p4	2.0	29.0224	40.9929	3	31	3.1	-1.8
p5	3.0	29.0236	40.9944	4	36	3.4	-2.8

Table 6.6. (Continued)

Name of Gauge Pt.	Depth (m)	Longitude (°)	Latitude (°)	Arrival time of initial wave (min)	Arrival time of max.wave (min)	Max. (+)ve amp. (m)	Max. (-)ve amp. (m)
p8	4.6	29.0197	40.9954	3	46	3.1	-2.7
p13	7.2	29.0171	40.9982	3	22	2.8	-4.6
p15	9.9	29.0144	41.0002	3	22	2.4	-4.2
p17	15.4	29.0117	41.0003	3	21	2.1	-4.3
p20	0.9	29.0103	41.0026	4	21	2.5	-0.9
p24	8.4	29.0124	41.0035	4	22	3.2	-4.9
p28	12.2	29.0084	41.0043	4	21	2.2	-4.2
p32	5.0	29.0067	41.0074	3	34	3.5	-3.4
p35	8.6	29.0094	41.0078	3	34	4.0	-6.0
p46	5.1	29.0088	41.0105	4	33	3.7	-3.4
p48	11.5	29.0041	41.0096	3	33	3.2	-6.1
p50	12.1	29.0063	41.0058	3	32	2.5	-4.8
p52	11.6	29.009	41.0013	3	21	3.1	-4.2
p53	11.3	29.0104	40.9994	3	21	2.1	-4.2
p55	5.3	29.0164	40.9966	4	17	2.1	-4.1
p58	5.9	29.0162	40.993	3	36	3.0	-5.9

6.4. Tsunami Analysis for Model 4

The tsunami parameters of Model 4 are computed near shorelines in Domain D by NAMI DANCE. The selected computed results are drawn in Table 6.7 and arrival time of initial and maximum tsunami waves and maximum positive and negative wave amplitudes at selected gauges are tabulated in Table 6.8.

Table 6.7. Computed tsunami parameters of Model 4
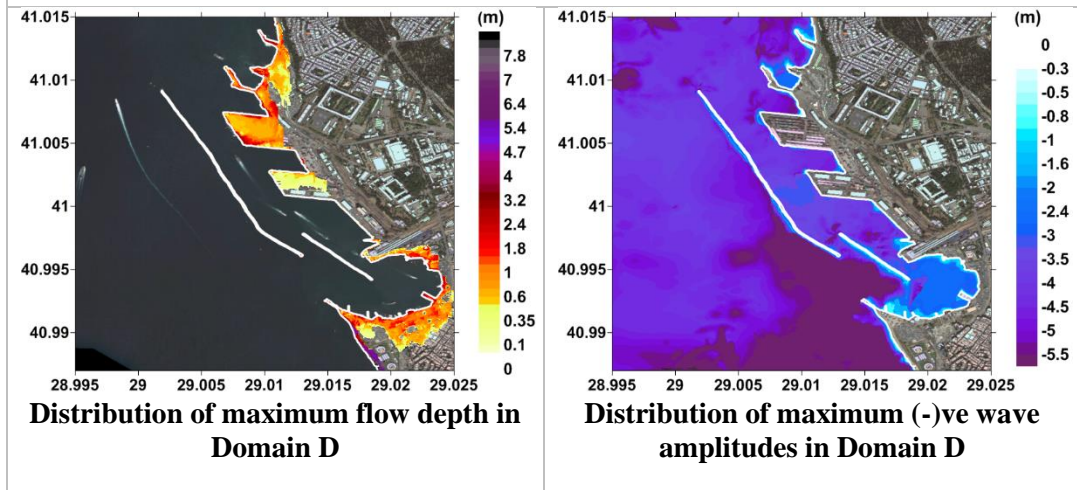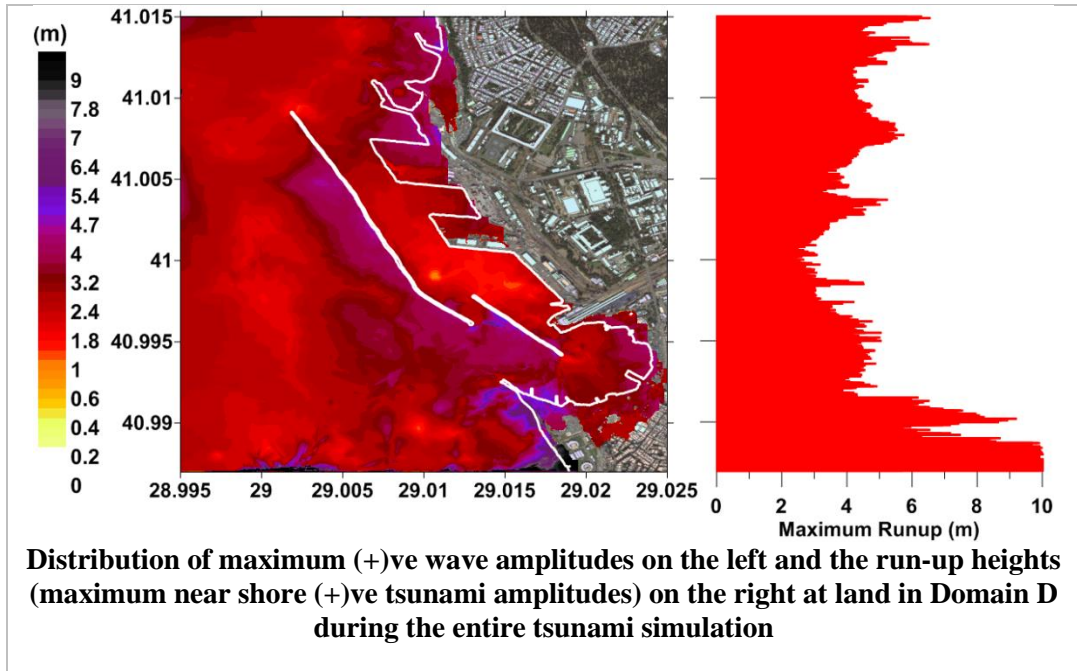
Distribution of maximum (+)ve wave amplitudes on the left and the run-up heights (maximum near shore (+)ve tsunami amplitudes) on the right at land in Domain D during the entire tsunami simulation

Distribution of maximum flow depth in Domain D

Distribution of maximum (-)ve wave amplitudes in Domain D

The maximum near shore positive tsunami amplitude	: 6.0 m
The minimum near shore negative tsunami amplitude	: -5.5 m
The maximum flow depth	: 4.8 m
Maximum inundation distance	: 350 m

Table 6.8. Maximum positive and negative wave amplitudes and arrival time of initial and maximum wave of Model 4 at selected numerical gauge points with their water depths and coordinates

Name of Gauge Pt.	Depth (m)	Longitude (°)	Latitude (°)	Arrival time of initial wave (min)	Arrival time of max.wave (min)	Max. (+)ve amp. (m)	Max. (-)ve amp. (m)
hp4	2.6	29.0162	40.9952	2	36	4.2	-2.5
hp6	-4.0	29.0167	40.9954	20	22	4.8	0.0
hp8	3.6	29.0169	40.9955	3	23	3.4	-3.2
hp11	3.9	29.0177	40.9958	3	37	2.8	-3.9
hp12	-2.4	29.0183	40.9959	37	37	2.8	0.0
hp14	-4.3	29.0191	40.9962	0	0	0.0	0.0
hp19	1.8	29.0187	40.997	3	24	2.6	-1.4
hp21	-2.9	29.0192	40.9971	37	37	2.9	0.0
hp23	-3.1	29.0194	40.9973	0	0	0.0	0.0
hp29	2.2	29.0222	40.9955	3	21	3.7	-2.2
hp30	2.0	29.0226	40.9958	3	21	3.8	-1.4
hp31	-2.4	29.0228	40.9959	21	21	4.0	0.0
hp32	-2.6	29.0231	40.9961	21	21	3.3	0.0
hp72	9.6	29.0095	40.9978	2	47	3.9	-6.5
hp82	-4.0	29.0099	40.998	47	47	4.4	0.0
hp87	9.7	29.0102	40.9981	3	22	2.8	-3.4
hp90	9.0	29.0024	41.0077	3	21	3.0	-4.0
hp92	-3.0	29.0029	41.0077	20	21	3.8	0.0
hp94	12.5	29.0036	41.0078	3	22	2.8	-3.9
hp95	4.1	29.0096	41.0074	3	22	4.3	-4.1
hp96	0.8	29.01	41.0073	4	22	4.5	-0.8
hp97	-2.7	29.0107	41.0071	23	29	4.1	0.0
hp98	-2.8	29.0112	41.0071	0	0	0.0	0.0
p2	4.2	29.0204	40.9917	3	21	3.3	-2.8
p4	2.0	29.0224	40.9929	3	21	3.4	-1.9
p5	3.0	29.0236	40.9944	3	21	4.1	-2.9

Table 6.8. (Continued)

Name of Gauge Pt.	Depth (m)	Longitude (°)	Latitude (°)	Arrival time of initial wave (min)	Arrival time of max.wave (min)	Max. (+)ve amp. (m)	Max. (-)ve amp. (m)
p8	4.5	29.0197	40.9954	3	37	2.5	-2.7
p13	7.3	29.0171	40.9982	3	39	1.9	-4.5
p15	9.8	29.0144	41.0002	3	24	1.9	-3.5
p17	15.6	29.0117	41.0003	3	23	2.0	-3.3
p20	0.7	29.0103	41.0026	3	23	2.3	-0.7
p24	8.1	29.0124	41.0035	3	23	3.2	-4.5
p28	12.2	29.0084	41.0043	3	22	2.3	-3.9
p32	-1.0	29.0067	41.0074	15	22	3.3	0.0
p35	8.8	29.0094	41.0078	3	22	4.2	-5.4
p46	5.0	29.0088	41.0105	4	22	3.1	-2.7
p48	11.5	29.0041	41.0096	3	22	2.7	-3.9
p50	12.1	29.0063	41.0058	3	22	2.9	-4.1
p52	11.7	29.009	41.0013	3	22	2.3	-3.2
p53	11.3	29.0104	40.9994	3	23	1.8	-3.4
p55	5.3	29.0164	40.9966	3	24	2.2	-4.0
p58	5.9	29.0162	40.993	2	20	3.3	-5.9

6.5. Tsunami Analysis for Model 5

The tsunami parameters of Model 5 are computed near shorelines in Domain D by NAMI DANCE. The selected computed results are drawn in Table 6.9 and arrival time of initial and maximum tsunami waves and maximum positive and negative wave amplitudes at selected gauges are tabulated in Table 6.10. The computed results of all available gauges in Model 5 are also attached to Table A.1 in Appendix A.

Table 6.9. Computed tsunami parameters of Model 5
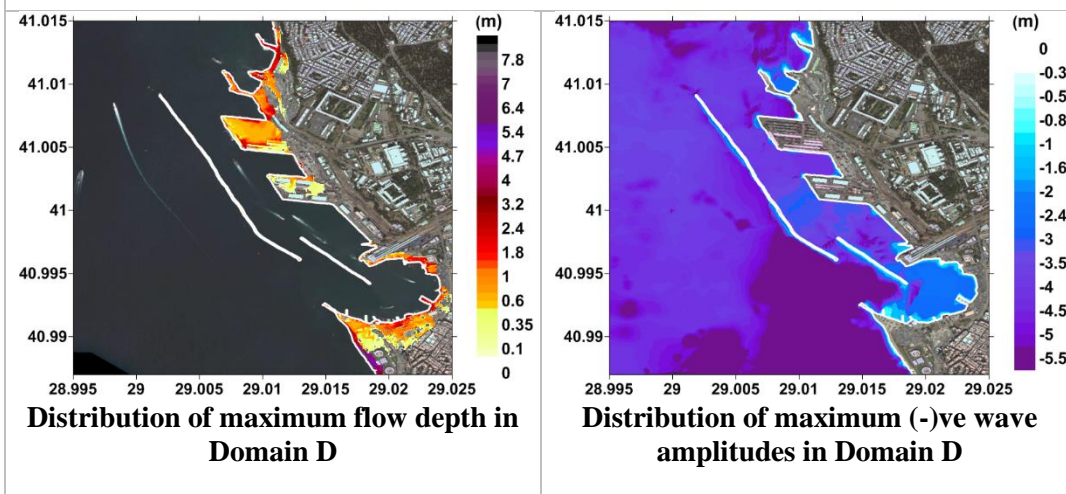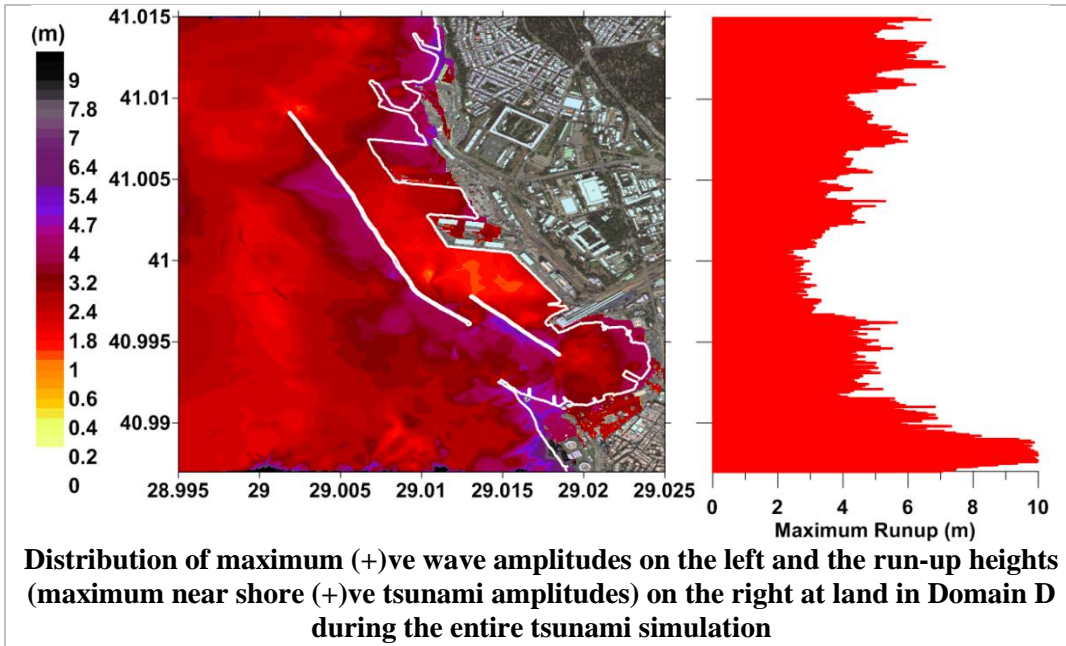
Distribution of maximum (+)ve wave amplitudes on the left and the run-up heights (maximum near shore (+)ve tsunami amplitudes) on the right at land in Domain D during the entire tsunami simulation

Distribution of maximum flow depth in Domain D

Distribution of maximum (-)ve wave amplitudes in Domain D

The maximum near shore positive tsunami amplitude	: 6.5 m
The minimum near shore negative tsunami amplitude	: -6.5 m
The maximum flow depth	: 4.8 m
Maximum inundation distance	: 340m

Table 6.10. Maximum positive and negative wave amplitudes and arrival time of initial and maximum wave at selected numerical gauge points with their water depths and coordinates

Name of Gauge Pt.	Depth (m)	Longitude (°)	Latitude (°)	Arrival time of initial wave (min)	Arrival time of max.wave (min)	Max. (+)ve amp. (m)	Max. (-)ve amp. (m)
hp4	2.5	29.0162	40.9952	2	27	4.7	-2.5
hp6	-3.1	29.0167	40.9954	20	46	4.8	0.0
hp8	3.6	29.0169	40.9955	3	36	3.7	-2.8
hp11	3.7	29.0177	40.9958	3	37	3.4	-3.4
hp12	-2.4	29.0183	40.9959	37	37	2.8	0.0
hp14	-9.3	29.0191	40.9962	0	0	0.0	0.0
hp19	3.2	29.0187	40.997	3	24	2.5	-1.4
hp21	-5.2	29.0192	40.9971	0	0	0.0	0.0
hp23	-3.1	29.0194	40.9973	0	0	0.0	0.0
hp29	2.5	29.0222	40.9955	3	21	3.7	-2.4
hp30	2.0	29.0226	40.9958	3	21	3.9	-1.4
hp31	-2.2	29.0228	40.9959	21	21	4.0	0.0
hp32	-10.7	29.0231	40.9961	0	0	0.0	0.0
hp72	9.4	29.0095	40.9978	2	47	4.3	-6.5
hp82	-4.0	29.0099	40.998	47	47	4.5	0.0
hp87	9.8	29.0102	40.9981	3	22	2.8	-3.2
hp90	9.1	29.0024	41.0077	3	21	2.9	-4.6
hp92	-3.0	29.0029	41.0077	21	47	3.4	0.0
hp94	12.5	29.0036	41.0078	3	22	2.7	-3.8
hp95	4.4	29.0096	41.0074	3	22	4.3	-4.4
hp96	0.7	29.01	41.0073	4	22	4.7	-0.7
hp97	-2.7	29.0107	41.0071	0	0	0.0	0.0
hp98	-2.8	29.0112	41.0071	0	0	0.0	0.0
p2	4.2	29.0204	40.9917	3	20	3.2	-2.6
p4	2.0	29.0224	40.9929	3	36	3.5	-1.9
p5	3.0	29.0236	40.9944	3	21	4.0	-2.6

Table 6.10. (Continued)

Name of Gauge Pt.	Depth (m)	Longitude (°)	Latitude (°)	Arrival time of initial wave (min)	Arrival time of max.wave (min)	Max. (+)ve amp. (m)	Max. (-)ve amp. (m)
p8	4.5	29.0197	40.9954	3	37	3.2	-2.3
p13	7.2	29.0171	40.9982	3	17	1.8	-3.6
p15	9.8	29.0144	41.0002	3	24	1.8	-3.2
p17	15.4	29.0117	41.0003	3	23	1.9	-3.2
p20	0.6	29.0103	41.0026	3	38	2.3	-0.6
p24	8.1	29.0124	41.0035	3	23	3.0	-4.1
p28	12.2	29.0084	41.0043	3	23	2.2	-3.8
p32	-0.9	29.0067	41.0074	15	22	3.3	0.0
p35	8.8	29.0094	41.0078	3	22	4.1	-5.3
p46	5.0	29.0088	41.0105	4	22	3.1	-2.6
p48	11.5	29.0041	41.0096	3	22	2.6	-3.8
p50	12.1	29.0063	41.0058	3	22	2.7	-3.6
p52	11.6	29.009	41.0013	3	38	2.1	-3.3
p53	11.3	29.0104	40.9994	3	23	1.5	-3.2
p55	5.3	29.0164	40.9966	3	39	1.9	-3.8
p58	6.0	29.0162	40.993	2	36	3.3	-5.9

CHAPTER 7

COMPARISONS AND DISCUSSIONS OF THE RESULTS

In this chapter, the results of all models presented in previous chapter are compared and discussed by considering different aspects.

Before the discussions, it is important to mention that the total area of the selected smallest study domains used in all models are about 7.85 km^2, of which about 2.74 km^2 is land area and 5.10 km^2 is sea area. Besides, all simulations in this study are performed by using computers with 64 processors (32 dual core). It means that NAMI DANCE performed all calculations by using all available processors of the executed computers.

7.1. Comparison of Model 1 and Model 2

Firstly, results of low resolution models, Model 1 and Model 2, are compared in terms of data resolution effect on the computed tsunami parameters. The bathymetric and topographic maps of these two models have same model resolution (10 m), but different data sets have been used during preparation of the models. The process time of each model is same, which is less than a day.

In Figure 7.1, tsunami inundation distances of two models are drawn for comparison. It is clearly seen from the figure that there is significant difference between inundation lines. As an example, there is highly inundated area on the bottom right of the topography obtained from Model 2 when it is compared with Model 1 results. It shows that elevations of Model 1 in this area is higher and tsunami waves can not penetrate to inner zones.

The inundated area in Model 1 is about 0.31 km^2, which equals 11.3% of total land area while the inundated area in Model 2 is about 0.47 km^2, which equals 17.0% of

total land area existing in this smallest domain. This shows that newly added data set led to an increase in inundated area almost 6%.
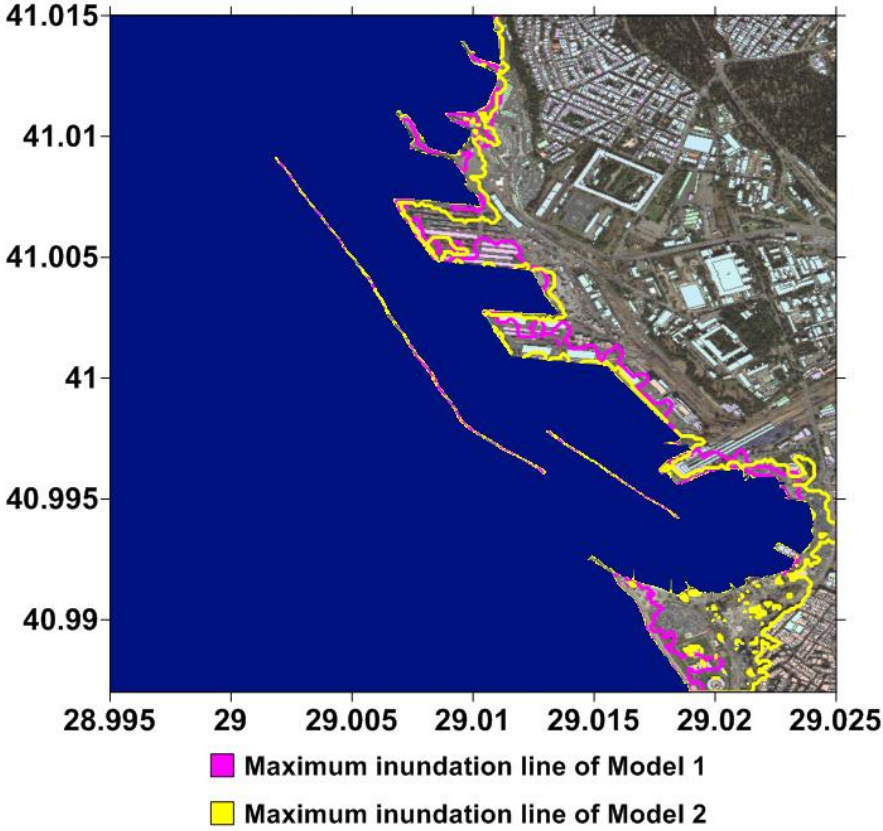
Figure 7.1. Comparison of tsunami inundation distances of Model 1 and 2

When the run-up plots of these two models presented in Table 6.1 and 6.3 are carefully examined, it is seen that maximum run-ups in Model 1 and Model 2 are around 4 m and 3 m, respectively, which also shows that Model 1 results in terms of maximum water elevations are higher in comparison to Model 2.

The conventional techniques to prepare topographic and bathymetric maps are using data from ASTER and GEBCO like in Model 1, since there may not always be an additional accurate data set available. However, the resolutions of these data sources are not high enough and this may cause change of real elevation values and corresponding inundations. Corrections on the shoreline usually are not sufficient. The availability of additional topographic data closer to the shoreline is very important.

According to these discussions, the traditional methods used to create bathymetric and topographic maps may prevent inundation to reach inner zones since topography gets higher just after the coastal line. This sudden increase in land elevations and change in bathymetric conditions may also cause an increase in maximum water elevation values inside the port and run-up values on land. In short, the reliability of the results directly depends on the resolution and accuracy of available data regarding the resolution of the model maps.

7.2. Comparison of Model 2 and Model 3

Secondly, results of Model 2 and Model 3 are compared in terms of model resolution effect. The bathymetric and topographic maps of these two models are created by using same data set and model runs performed by using rupture sources. The model resolutions of Model 2 and Model 3 are 10 m and 3 m, respectively. The process time of Model 2 is less than a day, while process time of Model 3 is over one and a half day.

In Figure 7.2, tsunami inundation distances of two models are drawn for comparison. When the figure is scrutinized, the slight local changes occur in inundation pattern. While inundations occur on lower part of the topography is quite close to each other in two models, they show differences on the upper part.

The inundated area in Model 2 is about 0.47 km^2, which equals 17.0% of total land area while the inundated area in Model 3 is about 0.57 km^2, which equals 20.6% of total land area existing in this smallest domain. This shows that higher model resolution led to an over 3% increase in inundated area. Even, differences in inundation lines occur, the result are quite close to each other.

When the run-up plots of these two models presented in Table 6.3 and 6.5 are carefully examined, it is seen that maximum run-ups in Model 2 and Model 3 are around 3 m and 5 m, respectively. The tables also show that Model 3 results in terms of maximum water elevations are higher in comparison to Model 2. This may be due to change in elevation values between two models. For example, since run-ups are higher right in

front of the structures and it is more possible to identify existing structures in Model 2, this model give higher run-up values.

1
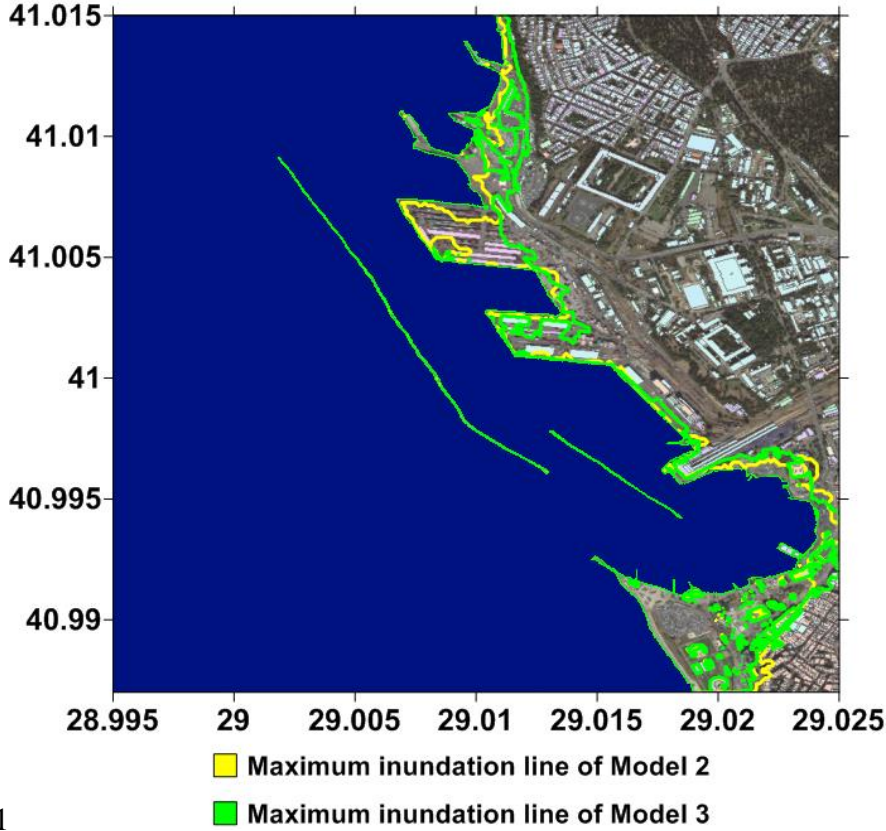
Figure 7.2. Comparison of tsunami inundation distances of Model 2 and 3

In short, when model resolution change, different values are interpolated to determine elevations on each grid. Therefore, even same data set has been used for these two models, elevations in maps are not identical. This elevation change may cause different calculated tsunami parameters. However, it may be still said that results obtained from lower model resolutions by using same data set are in acceptable limits according to Model 2 and Model 3 results. On the other hand, if more accurate and reliable results are needed and data with sufficient resolution is available, it is better to prepare models in high resolution.

7.3. Comparison of Model 4 and Model 5

Thirdly, results of two high resolution models run with border source, Model 4 and Model 5, are compared. The bathymetric and topographic maps of these two models

are created by using same data set and model runs performed by using border sources. Both models have 1 m model resolution. The process time of these models is same, which is three days.

In Figure 7.3, tsunami inundation distances of two models are drawn for comparison. Modified situation of buildings changed the inundation pattern as it can be seen from the figure. The inundated area in Model 4 is about 0.52 km^2, which equals 18.8% of total land area while the inundated area in Model 5 is about 0.42 km^2, which equals 15.3% of total land area existing in this smallest domain. This shows that placing of structures in real dimension (Model 5) which minimizes smoothing due to interpolation led to a decrease in inundated area over 3%. According to these results it is possible to say that when buildings are placed specifically as elevation data, it is eventuated a decrease of inundation extent. This occurs due to the resistance of available structures, which reduce the water flow into the land area.
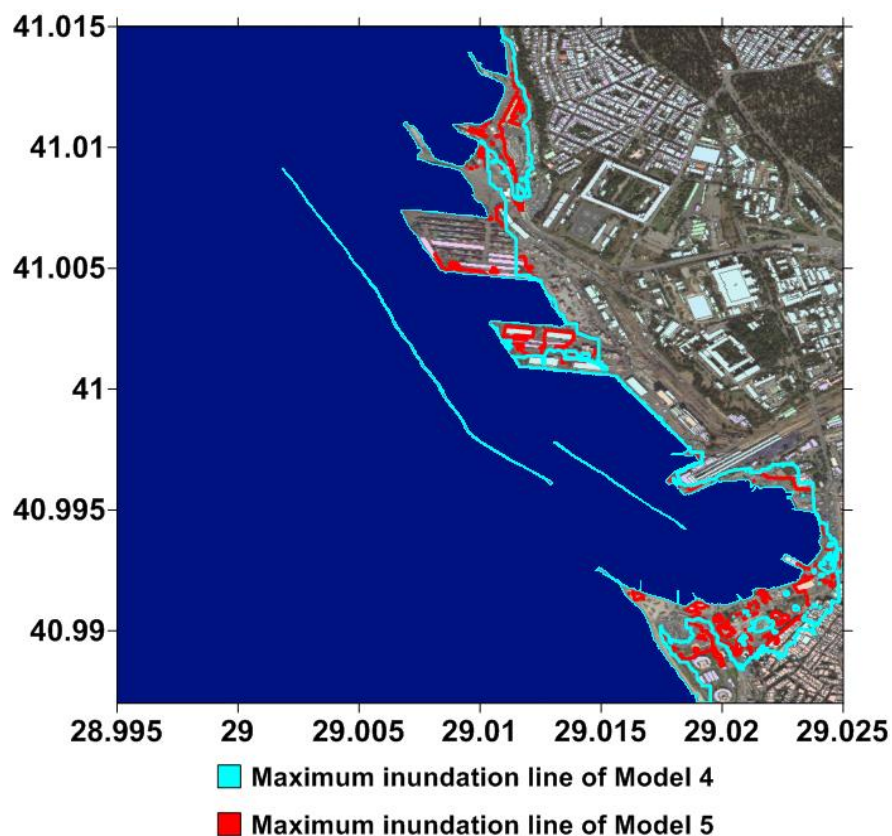
Figure 7.3. Comparison of tsunami inundation distances of Model 4 and 5

For detailed analysis on effect of the structures existing in the area, three different profiles are selected (Profile A, B and C) and shown in Figure 7.4. In the figure, the change of ground elevation, maximums of flow depth and current velocity on land along the profile axis A, B and C are also plotted. It should also be indicated here that existing structures are rigid (undamaged) and impermeable (no penetration through the windows is allowed).

According to elevation graphs, it is seen that there are obvious changes in elevations between two models where structures are existing. Correspondingly, differences occur on values of maximum flow depths and currents on land. When the maximum flow depth on land plots of Model 4 and Model 5 are compared, the larger flow depths are observed right in front of the existing structures in Model 5 because of accumulation of water volume in front of rigid structures. However, flow depths are zero on the land structures as long as no overtopping observed. Likewise, similar behavior of maximum current velocities on land are noticed at identical locations due to relationship between flow depths and currents for long waves.

When structures are not placed specifically to topographic map as elevation data, smoothing or even neglecting of elevations may occur. Hence, the results may also be smoothed. To avoid this effect, it is important to define structures especially the ones near coastal zones when results at specific points are needed to be analyzed.
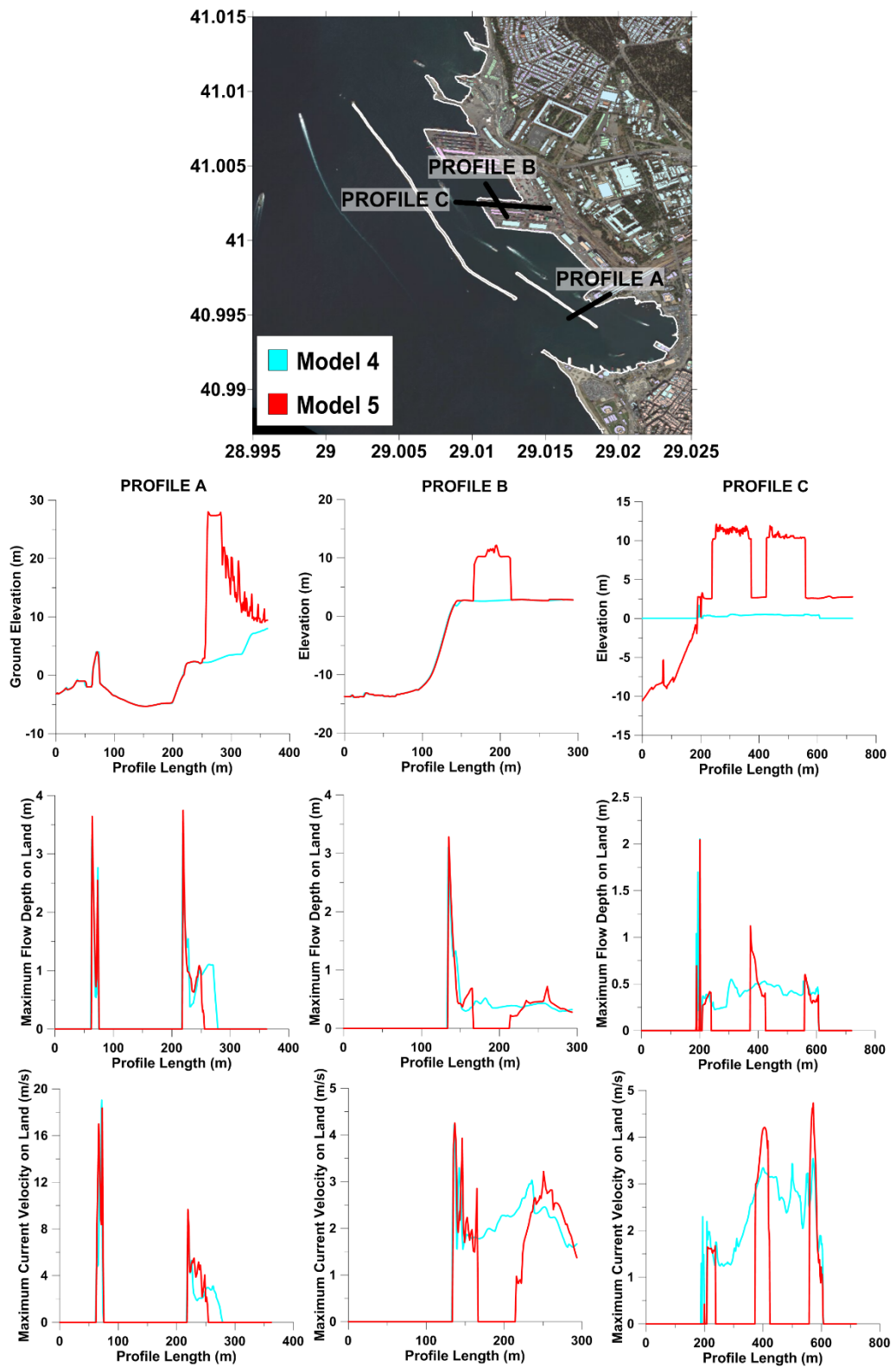
Figure 7.4. The ground elevation change, maximum flow depth on land and maximum current velocity on land plots of models at selected profiles

7.3. Comparison of Model 3 and Model 5

Fourthly, results of Model 3 and Model 5 are compared. For both models, same data sets used during preparation of maps but smallest chosen domains have different model resolutions as 3 m and 1 m.

Herein it is important to remind that rupture source is used for Model 3 simulations and border source is used for Model 5 simulations. For a better comparison, another model with 1 m resolution map is prepared to be performed with a rupture source. However, process time of that model is almost 52 days whereas process time of Model 5 is about 3 days. As being the result of time limitation, the simulation results of that model could not be presented in this study.
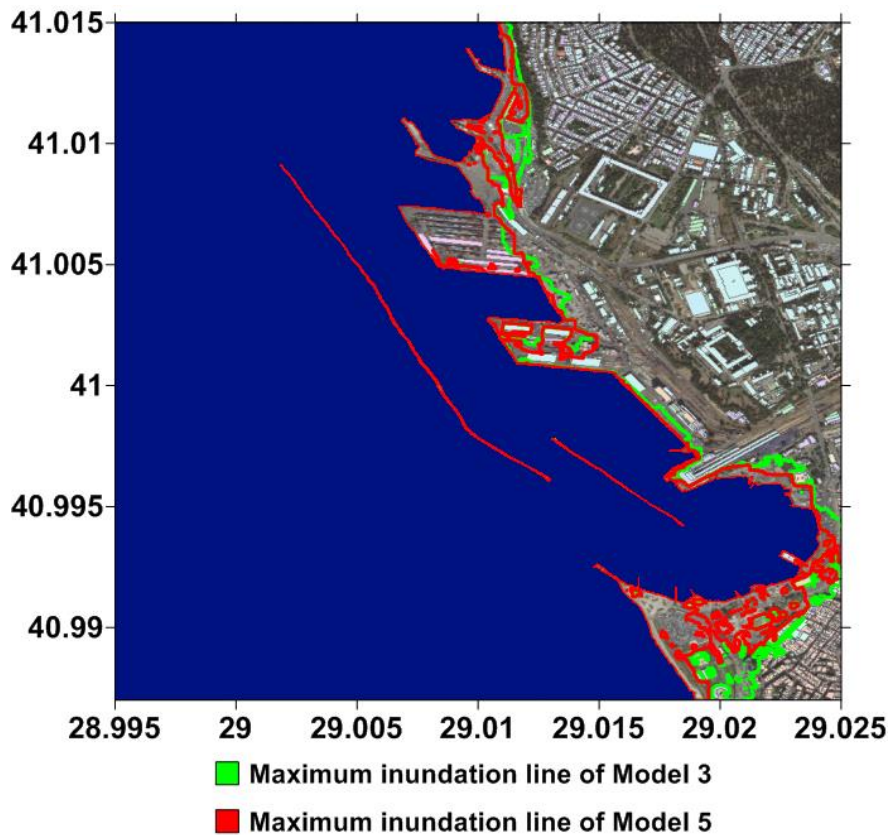
Figure 7.5. Comparison of tsunami inundation distances of Model 3 and 5

In Figure 7.5, tsunami inundation distances of two models are drawn for comparison. It should be indicated here that this comparison should be considered as a rough comparison since the input of sources are different type. It is seen that inundated area slightly differs in both models. The inundated area in Model 3 is about 0.57 km^2, which

equals 20.6% of total land area while the inundated area in Model 5 is about 0.42 km^2, which equals 15.3% of total land area existing in this smallest domain. This shows that decrease in model grid size led to a decrease in inundated area over 5%. This difference between inundated areas mainly comes from the inundation difference on the lower part of the maps.

When the run-up plots of these two models presented in Table 6.5 and 6.9 and presented results at selected gauges in Table 6.6 and Table 6.10 are carefully examined, it is seen that maximum run-ups in Model 3 and Model 5 are around 5 m while considerable run-up variations are observed in Model 5.

The reason of these changes in calculated tsunami parameters may be the border source. It is the time series recorded at a selected point on the border and it is assumed to represent time series of all points on the border. In addition, the direction information is not used. Therefore, the source is assumed to be perpendicular to the border.

Even, differences in inundation lines and calculated tsunami parameters occur between these two models, the results are still quite close to each other except the area near the bottom border. This area is close to border and could be influenced by the boundary effect in both model. When that small area ignored, the inundated areas in Model 3 and Model 5 equal 18.5% and 14.7% of total new land area existing in this new smallest domain. The change in total inundated areas disregarding that area is less than 4%. Hence, it may be said that Model 3 and Model 5 results are compatible with each other and have sufficient model resolution and adequate data set to accurately solve possible tsunami wave behavior in the selected region if rapid results are needed.

7.5. Tsunami Risk Assessment of Haydarpasa Port

The most reliable and accurate results are obtained from Model 3 and 5. Since Model 5 results are based on highest resolution, those are used in tsunami risk assessment studies hereafter. Figure 7.6 shows the final aerial view of Haydarpasa Port prepared in NAMI DANCE with distribution of maximum flow depths on land.

Figure 7.6. Distribution of maximum flow depth on land with the aerial view of Haydarpasa Port

According to Table 6.9 and Table 6.10 presented in previous chapter, it is seen that initial tsunami wave reached the port area in 5 minutes. After 20 minutes, the maximum tsunami wave observed in the port area. Considering the run-up plot of Model 5 given in Table 6.9, maximum run-up values change between 4.5 m and 6 m principally. In addition, time histories of current velocity at some selected gauge points given in Figure 7.7. As seen from the figure that, the current velocities at selected gauge points are in the range between 2-4 m/sec except the gauges "p55" and "p8" where maximum current velocity reaches 7-8 m/sec.

It is also important to state here that the computed values in Table 6.10 does not cover the possible change of water level in long term and short term rise of water due to wind, wave and barometric effects (setup) during the storm and surge conditions if occur during tsunami in general.

The concluded remarks according to obtained results are as follows:

- The two breakwaters available in the selected region reduce effect of tsunami waves on the coast and damage on port environs. However, wave overtopping was observed on breakwaters after a while. It is possible that this overtopping discharge will damage breakwaters and affect their stability. This may lead to an increase in tsunami inundation extent presented in this study.

74
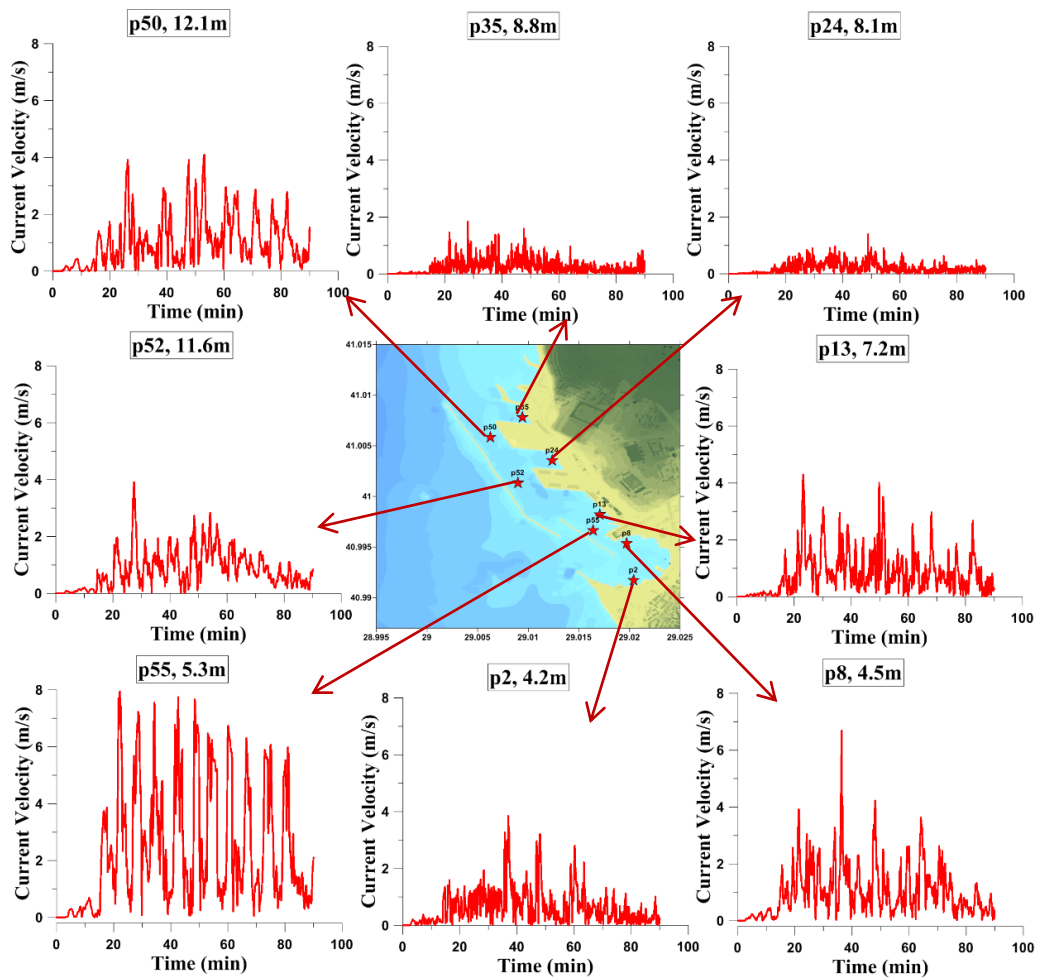
Figure 7.7. Time histories of current velocity at some selected gauge

- Higher run-up values are observed at the corners of inner (rhombohedron shaped) basins. They trap water volume inside and cause additional water level increase inside the inner basins.

- The current velocities exceed 6 m/sec at some locations especially in the region bounded by two parallel breakwaters and at the entrance of the circular basin. Current velocities are also high around the breakwaters, which may cause scouring at the toe of the coastal structures.

- The simulation show that the water flow parallel to the breakwaters during tsunami attack occurred.

- Some structures located near shoreline may partially damage as being the result of the impact forces applied by tsunami waves.

75

- Damages and dragging of floating bodies, such as cargo vessels or ferries, due to strong currents and water level rise at the port should be expected. Likewise, they can damage to same structures near coastal line.

- Since the port is the largest container port in Marmara region, a great number of containers are usually situated in different parts of it. High current velocities are especially occurred on rhombohedron shaped parts of the port. Thus, the containers in this area can also be floated and dragged.

- The selected study area is an urbanized area and hosts many structures in the coastal zone. It should be reminded that current velocities might increase in between the solid structures because of channel effect. For example, two storage buildings of the port are located on rhombohedron shaped part in parallel with each other as seen in Figure 7.8. Two different profiles are taken to examine the channel effect. One of the profiles is taken from right next to the storage buildings and other one is taken along the storage buildings. According to given graphs in the figure it is possible to say that current velocities are higher between storage buildings as it is expected.
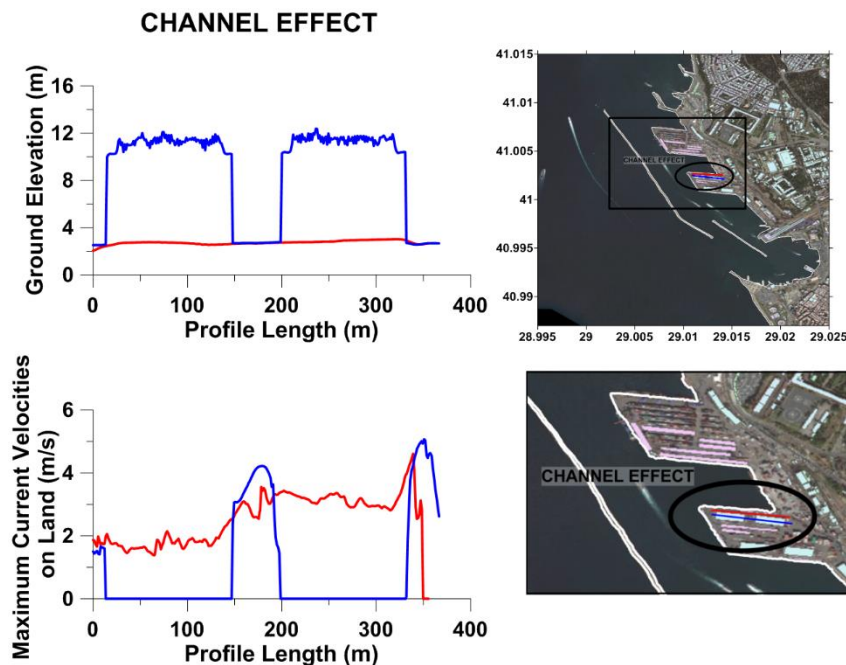
Figure 7.8. The ground elevation change and maximum current velocity on land plots at selected profiles

76

- Even if the simulation results do not show wave penetration to railway lines at Haydarpasa Train Station, it is also recommended that protection structures (walls, dikes) against tsunami inundation have to be considered to prevent unexpected damages on transportation elements at the station (See Figure 7.9).

- Although this thesis is focused on Haydarpasa Port, the arc shaped bay at south of the port near Kadikoy is also another important area. Because there are intercity passenger and ferry terminals, which serves one of the important business districts of Istanbul at Kadikoy. This area is highly inundated according to simulation results. It indicates that tsunami hazard analysis specifically for Kadikoy district is also necessary (See Figure 7.9).
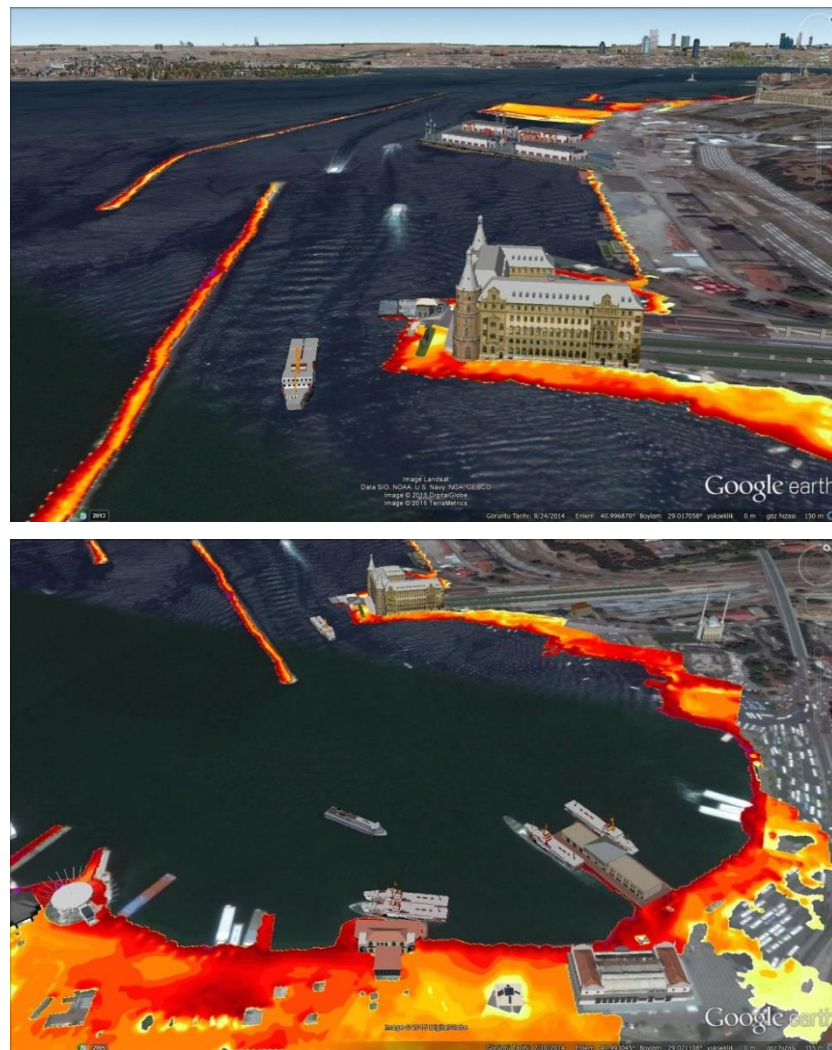
Figure 7.9. 3D view of tsunami inundation at Haydarpasa and Kadikoy region

In short, it is also possible to say that such a tsunami will negatively affect this urbanized area by considering economic and social aspects.

CHAPTER 8

CONCLUSION AND SUGGESTIONS FOR FURTHER STUDIES

In this study, a series of numerical computation was performed for Haydarpasa Port in the Sea of Marmara by using NAMI DANCE. The change in data and model resolution in different application methods for numerical modeling is discussed together with an assessment study for the selected port.

In light of the results obtained, the author recommends that data acquisition only from ASTER and GEBCO should be avoided as much as possible in order to determine tsunami inundation extent or measure other tsunami parameters. This traditional method may lead to underestimation of inundation extents. It is very important to determine inundation extent accurately in disaster management applications since evacuation plans are prepared according to these results.

The results presented in this study also showed that when existing structures in the study domain are not placed specifically as elevation data, smoothing of the elevations in DEMs followed by smoothing of the results might occur. Correspondingly, calculated hydrodynamic values such as flow depths and velocities may change especially in front of the structures. When decision makers require calculation of tsunami parameters at specifically defined points in urban areas, this smoothing of the results may be misleading.

When the initial tsunami source is inputted as a border source, overestimation or underestimation of inundation extents may occur according to chosen border gauge and corresponding time series of water surface elevation. However, such method significantly decreases the process time of high resolution simulations to more feasible levels. It should be reminded that overestimation of inundation extent may be considered being on the safe side as long as it is in reasonable limits.

Although, highest resolution simulations provide the most accurate and reliable results for decision makers, it is also concluded in this study that it is not always required to increase model resolution to highest level. Proper model resolution according to needs of the decision makers may be acceptable as long as the original data has sufficient resolution. Particularly, if there exist time limitations, study with high resolution models is not usually applicable. Increase in software techniques and hardware technology will certainly provide the researchers to perform highest resolution simulations by increasing simulation speed and reducing required time. Hence, results of these simulations will give correct inputs to decision makers.

Eventually, among all the results obtained from models, Model 5 results are used for assessment studies of Haydarpasa Port in this study. It is clear that, the water area inside the port will be agitated and water flow parallel to breakwaters will occur concerning functions of port. This behavior will cause amplification of water level and current velocities inside the port. Damages and dragging of floating bodies due to strong currents and water level rise at the port should also be expected.

During this study, the friction effect on calculated tsunami parameters was ignored. It is suggested that further studies should be performed by defining proper Manning's coefficient scheme for all topography. After that, it is possible to discuss the effect of friction on calculated tsunami parameters. It is also possible to consider vegetation in the selected area in order that presence of vegetation may prevent the tsunami waves to penetrate inner zones and change inundation extent.

Resilience of Haydarpasa Port after a disaster is important for Istanbul. Main requirement to enhance the resilience of Haydarpasa Port is to strengthen the two breakwaters to be undamaged against tsunami. Hence, less amplification inside the port and less inundation at the area of cargo handling and storage facilities could be obtained. The port operations could not be interrupted.

In addition, vulnerability analysis of the port and its surrounding area can be performed in future studies, since high resolution map of this region is available with the detailed structure information.

REFERENCES

Advanced Spaceborne Thermal Emission and Reflectance Radiometer (ASTER), Global Digital Elevation Model Version 2 (GDEM V2) (2011). Retrieved 20 June 2014, from http://gdex.cr.usgs.gov/gdex/.

Altinok, Y., Alpar, B., Ozer, N., and Gazioglu, C. (2011). *Revision of the tsunami catalogue affecting Turkish coasts and surrounding regions*, Nat. Hazards Earth Syst. Sci., 11, 273–291, doi: 10.5194/nhess-11-273-2011.

Armijo, R., Pondard, N., Meyer, B., Uçarkus, G., de Lépinay, B., and Malavieille, J. et al. (2005). *Submarine fault scarps in the Sea of Marmara pull-apart (North Anatolian Fault): Implications for seismic hazard in Istanbul*. Geochemistry, Geophysics, Geosystems, 6(6), n/a-n/a. doi:10.1029/2004gc000896.

Ayca, A. (2012). *Development of a Web GIS-Based Tsunami Inundation Mapping Service; A Case Study For Marmara Sea Region*, Master of Science Thesis, Middle East Technical University, Department of Civil Engineering, Ocean Engineering Research Center, Ankara, Turkey.

Aydın, D. I. (2014). *Tsunamis Generated by Submarine Landslides in the Marmara Sea*, Master of Science Thesis, Boğaziçi University, Kandilli Observatory and Earthquake Research Institute, Istanbul, Turkey.

Aytore, B., Acar, S., Yalciner, A. C. and Zaytsev, A. (2013). *Assessment of Tsunami Resilience Of Ports By High Resolution Numerical Modeling; A Case Study for Haydarpasa Port in the Sea of Marmara*, Proceedings of 26th International Tsunami Symposium (pp. 135). Gocek, Turkey.

Aytore, B., Cankaya, Z. C., Yalciner, A. C., Suzen, M. L., and Zaytsev, A. (2014). *High resolution data processing and tsunami assessment and applications to ports in the Sea of Marmara*. In Mega Earthquakes and Tsunamis in Subduction Zones– Forecasting Approaches and Implications for Hazard Assessment (p. 19). Rhodes Isl., Greece.

Bryant, E. (2008). *Tsunami the Underrated Hazard* (2nd ed., Vol. Digital). Berlin, Heidelberg: Praxis Pub., Chichester, UK.

Dilmen, D. I. (2009). *GIS Based Tsunami Inundation Maps: Case Studies from Mediterranean*, Master of Science Thesis, Middle East Technical University, Department of Civil Engineering, Ocean Engineering Research Center, Ankara, Turkey.

Dilmen, D. I., Kemec, S., Yalciner, A. C., Duzgun, S., and Zaytsev, A. (2014). *Development of a Tsunami Inundation Map in Detecting Tsunami Risk in Gulf of Fethiye, Turkey*, Pure and Applied Geophysics, doi: 10.1007/s00024-014-0936-2.

General Bathymetric Chart of the Oceans, GEBCO_08 Grid (Version 20100927) (2010). Retrieved 20 June 2014, from http://www.gebco.net.

Hébert, H., Schindelé, F., Altinok, Y., Alpar, B., and Gazioglu, C. (2005). *Tsunami hazard in the Marmara Sea (Turkey): a numerical approach to discuss active faulting and impact on the Istanbul coastal areas*. Marine Geology, 215(1-2), 23-43. doi:10.1016/j.margeo.2004.11.006.

Imamura, F., and M.M.A. Imteaz. (1995). *Long waves in two-layers: Governing equations and numerical model*, Science of Tsunami Hazards 13:3–24.

Istanbul Metropolitan Municipality (2009), *Population and Demographic Structure*. Retrieved 25 December 2014, from http://www.ibb.gov.tr/sites/ks/en-US/0-Exploring-The-City/Location/Pages/PopulationandDemographicStructure.aspx.

Insel, I. (2009). *The Effects of the Material Density and Dimensions of the Landslide on the Generated Tsunamis*, Master of Science Thesis, Middle East Technical University, Department of Civil Engineering, Ocean Engineering Research Center, Ankara, Turkey.

Kaiser, G., Scheele, L., Kortenhaus, A., Løvholt, F., Römer, H., & Leschka, S. (2011). *The influence of land cover roughness on the results of high resolution tsunami inundation modeling*. Natural Hazards And Earth System Science, 11(9), 2521-2540. doi:10.5194/nhess-11-2521-2011.

Kaiser, G., Scheele, L., Kortenhaus, A., Løvholt, F., Römer, H., and Leschka, S. (2011). *The influence of land cover roughness on the results of high resolution tsunami inundation modeling*, Natural Hazards And Earth System Science, 11(9), 2521-2540. doi:10.5194/nhess-11-2521-2011.

NAMI DANCE (2011). *Manual of Numerical Code NAMI DANCE*. Retrieved 15 October 2014, from http://namidance.ce.metu.edu.tr.

Necmioğlu, O., & Ozel, N. (2014). *An Earthquake Source Sensitivity Analysis for Tsunami Propagation in the Eastern Mediterranean*. Oceanog, 27(2), 76-85. doi:10.5670/oceanog.2014.42

Oliver, M., and Webster, R. (2014). *A tutorial guide to geostatistics: Computing and modeling variograms and kriging*. CATENA, 113, 56-69. doi:10.1016/j.catena.2013.09.006

Onat, Y. (2011). *Database Development for Tsunami Warning System in Mediterranean Basin by Tsunami Modeling*. Master of Science Thesis, Middle East Technical University, Department of Civil Engineering, Ocean Engineering Research Center, Ankara, Turkey.

Onat, Y. and Yalciner, A. C. (2013). *Initial Stage of Database Development for Tsunami Warning System along Turkish Coasts*, Ocean Engineering. Vol. 74, 141-154. doi: 10.1016/j.oceaneng.2013.09.008.

OYO and IMM (2007). *Simulation and Vulnerability Analysis of Tsunamis Affecting the Istanbul Coasts*, Project report performed for Istanbul Metropolitan Municipality by Oyo Int. Co, Japan.

Ozdemir, K. K. (2014). *Database Development For Tsunamı Informatıon System*. Master of Science Thesis, Middle East Technical University, Department of Civil Engineering, Ocean Engineering Research Center, Ankara, Turkey.

Ozel, N., Ocal, N.,Yalciner, A. C., Kalafat, D., Erdik, M. (2011). *Tsunami Hazard in the Eastern Mediterranean and Its Connected Seas: Toward a Tsunami Warning Center in Turkey.* Soil Dynamics and Earthquake Engineering, 31, 598–610.

Ozer, C. (2012). *Tsunami Hydrodynamics in Coastal Zones*, Doctor of Philosophy Thesis, Middle East Technical University, Department of Civil Engineering, Ocean Engineering Research Center, Ankara, Turkey.

Pamuk, A. (2014), *Assessment of Inland Tsunami Parameters and Their Effects on Morphology*, Master of Science Thesis, Middle East Technical University, Department of Civil Engineering, Ocean Engineering Research Center, Ankara, Turkey.

Papadopoulos G. A., Gracia, E., Urgeles, R., Sallares, V., De Martini, P. M., Pantosti, D., Gonzalez, M., Yalciner, A. C., Mascle, J., Sakellariou, D., Salamon, A., Tinti, S., Karastathis, V., Fokaefs, A., Camerlenghi, A., Novikova, T., Papageorgiou, A. (2014). *Historical and Pre-historical Tsunamis in the Mediterranean and Its connected Seas: Geological Signatures, Generation Mechanisms and Coastal Impacts*. Marine Geology 354: 81-103. doi: 10.1016/j.margeo.2014.04.014.

Şafak, C. (2010). *Haydarpaşa'da Hayat.* In Kuruluş Yıllarında Haydarpaşa Sendikası (1950-1964) (Vol. 1, p. 25). İstanbul : TÜSTAV.

Turkish Statistical Institute (2014). *Population and Demography*. Retrieved 17 December 2014, from http://www.turkstat.gov.tr/UstMenu.do?metod=temelist

Ünlü, S. (2007). *Comparative Analytical Data in the Source Determination of Unknown Spilled Oil in the Haydarpaşa Port (Marmara Sea), Turkey*. Bull Environ Contam Toxicol, 78(5), 363-367. doi:10.1007/s00128-007-9199-2.

Yalciner, A.C., Alpar B., Altınok Y., Özbay İ. and Imamura F. (2002). *Tsunamis in the Sea of Marmara: Historical documents for the past, models for the future*. Marine Geology 190:445–463, doi: 10.1016/S0025-3227(02)00358-4.

Yalciner, A.C., Zaytsev, A., Aytore, B., Insel, I., Heidarzadeh, M., Kian, R. and Imamura, F. (2014). *A possible submarine landslide and associated tsunami at the Northwest Nile Delta, Mediterranean Sea*. Oceanography 27(2):68–75, doi: 10.5670/oceanog.2014.41.

Yalciner A.C., Gülkan P., Dilmen D.I., Aytore B., Ayca A., Insel I. and Zaytsev A. (2014). *Evaluation of tsunami scenario for western Peloponnese, Greece*. Boll. Geof. Teor. Appl., 55, 485-500, doi:10.4430/bgta0126.

Zitter, T.A.C., Grall, C., Henry, P., Ozeren, M.S., Çagatay, M.N., Sengor, A.M.C., Gasperini, L., Mercier de Lépinay, B. and Géli, L. (2012). *Distribution, morphology and triggers of submarine mass wasting in the Sea of Marmara*. Marine Geology 329-331: 58-74. doi: 10.1016/j.margeo.2012.09.002.

APPENDICES

MODEL 5 SUMMARY OF RESULTS

In Figure A.1, all gauge points are given used in simulations. The detailed list of selected gauges with their coordinate information and depths and, obtained NAMIDANCE results after simulation of each model at those gauges are given in tables. These results includes arrival time of the initial and maximum tsunami wave to each selected gauge and maximum positive and negative wave amplitudes at those locations.
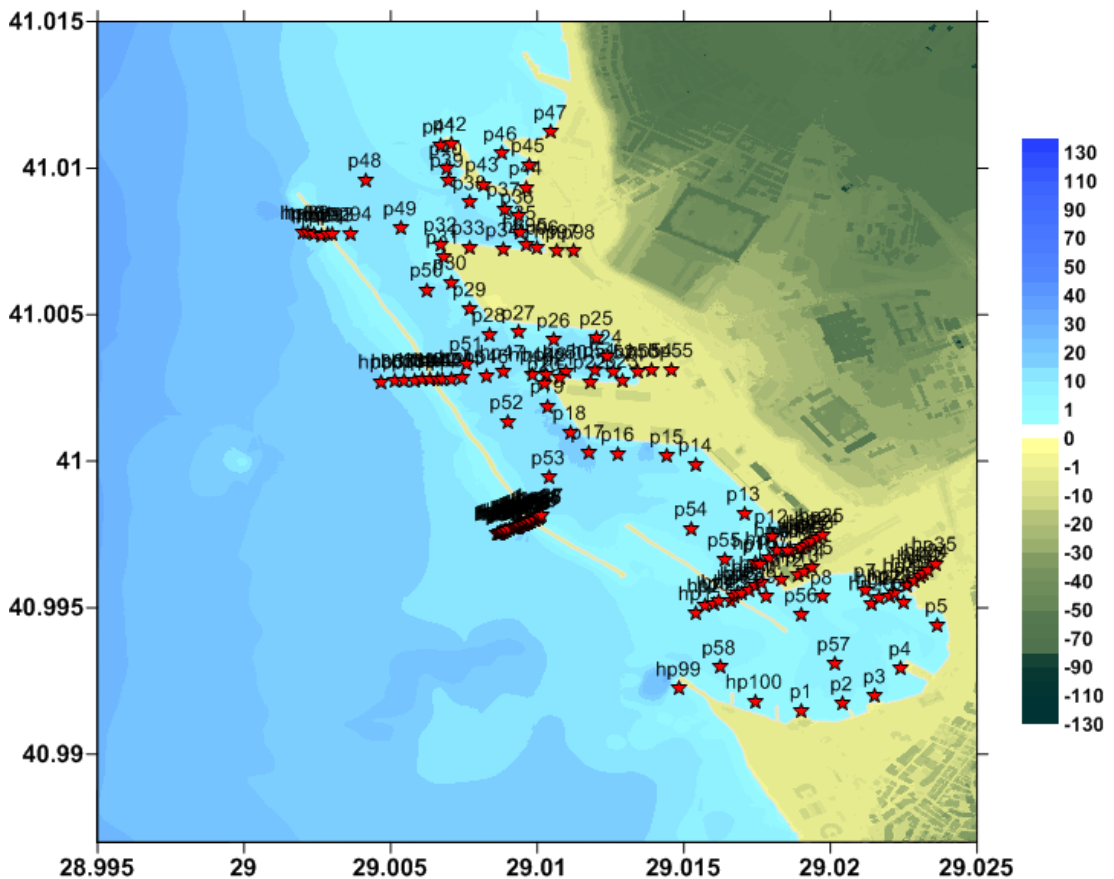
Figure A.1. The general view of all numerical gauge points used in simulations

A.1. Full List of Model 5 Simulation Results

NAMIDANCE results after simulation of Model 5 at all gauges are given in Table A.1.

Table A.1. Summary sheet of the simulation results of Model 5

Name of Gauge Pt.	Depth (m)	Longitude (°)	Latitude (°)	Arrival time of initial wave (min)	Arrival time of max.wave (min)	Max. (+)ve amp. (m)	Max. (-)ve amp. (m)
hp1	7.4	29.0154	40.9948	2	35	3.5	-6.2
hp2	6.3	29.0157	40.9951	2	36	3.6	-6.2
hp3	4.3	29.016	40.9951	2	46	4.7	-4.3
hp4	2.5	29.0162	40.9952	2	27	4.7	-2.5
hp5	1.0	29.0166	40.9952	2	46	4.9	-0.9
hp6	-3.1	29.0167	40.9954	20	46	4.8	0.0
hp7	2.7	29.0168	40.9955	3	36	3.7	-2.7
hp8	3.6	29.0169	40.9955	3	36	3.7	-2.8
hp9	4.9	29.0172	40.9956	3	36	4.0	-2.7
hp10	5.3	29.0174	40.9957	3	36	3.5	-2.9
hp11	3.7	29.0177	40.9958	3	37	3.4	-3.4
hp12	-2.4	29.0183	40.9959	37	37	2.8	0.0
hp13	-16.6	29.0189	40.9961	0	0	0.0	0.0
hp14	-9.3	29.0191	40.9962	0	0	0.0	0.0
hp15	-9.4	29.0193	40.9964	0	0	0.0	0.0
hp16	4.2	29.0175	40.9965	3	37	2.6	-3.9
hp17	1.1	29.0179	40.9967	3	24	2.5	-1.1
hp18	2.0	29.0182	40.997	3	24	2.3	-1.6
hp19	3.2	29.0187	40.997	3	24	2.5	-1.4
hp20	0.0	29.019	40.997	10	48	2.8	0.0
hp21	-5.2	29.0192	40.9971	0	0	0.0	0.0
hp22	-9.4	29.0193	40.9972	0	0	0.0	0.0
hp23	-3.1	29.0194	40.9973	0	0	0.0	0.0
hp24	-2.5	29.0196	40.9974	0	0	0.0	0.0
hp25	-3.0	29.0197	40.9975	0	0	0.0	0.0

Table A.1. (Continued)

Name of Gauge Pt.	Depth (m)	Longitude (°)	Latitude (°)	Arrival time of initial wave (min)	Arrival time of max.wave (min)	Max. (+)ve amp. (m)	Max. (-)ve amp. (m)
hp26	3.9	29.0214	40.9951	3	21	3.2	-2.3
hp27	2.4	29.0217	40.9953	3	21	3.4	-2.4
hp28	2.6	29.022	40.9954	3	21	3.6	-2.6
hp29	2.5	29.0222	40.9955	3	21	3.7	-2.4
hp30	2.0	29.0226	40.9958	3	21	3.9	-1.4
hp31	-2.2	29.0228	40.9959	21	21	4.0	0.0
hp32	-10.7	29.0231	40.9961	0	0	0.0	0.0
hp33	-11.5	29.0232	40.9962	0	0	0.0	0.0
hp34	-12.0	29.0233	40.9963	0	0	0.0	0.0
hp35	-2.6	29.0236	40.9965	0	0	0.0	0.0
hp36	15.3	29.0047	41.0027	2	20	3.6	-4.5
hp37	13.7	29.0051	41.0027	2	20	3.6	-4.6
hp38	12.2	29.0055	41.0027	2	20	3.7	-4.7
hp39	9.9	29.0058	41.0027	2	20	4.0	-4.9
hp40	5.8	29.0061	41.0028	2	20	4.1	-5.2
hp41	4.0	29.0063	41.0028	2	20	4.2	-2.7
hp42	1.0	29.0066	41.0028	3	22	2.7	-0.9
hp43	9.1	29.0068	41.0028	3	22	2.4	-3.9
hp44	11.6	29.0071	41.0028	3	22	2.2	-3.8
hp45	11.8	29.0075	41.0029	3	22	2.1	-3.8
hp46	12.4	29.0083	41.0029	3	23	2.1	-3.8
hp47	12.2	29.0088	41.003	3	23	2.2	-3.9
hp48	6.7	29.0098	41.003	3	23	2.3	-3.9
hp49	3.0	29.0103	41.003	3	38	2.7	-3.0
hp50	9.4	29.011	41.003	3	38	3.0	-4.2
hp51	13.6	29.012	41.0031	3	38	3.1	-4.2
hp52	5.5	29.0126	41.003	3	38	3.5	-4.3

Table A.1. (Continued)

Name of Gauge Pt.	Depth (m)	Longitude (°)	Latitude (°)	Arrival time of initial wave (min)	Arrival time of max.wave (min)	Max. (+)ve amp. (m)	Max. (-)ve amp. (m)
hp53	-1.8	29.0134	41.0031	21	38	4.2	0.0
hp54	-2.7	29.0139	41.0031	0	0	0.0	0.0
hp55	-2.8	29.0146	41.0031	0	0	0.0	0.0
hp56	9.8	29.0086	40.9975	2	47	3.3	-5.9
hp57	9.9	29.0087	40.9975	2	47	3.4	-6.0
hp58	9.6	29.0087	40.9975	2	47	3.4	-6.0
hp59	9.5	29.0087	40.9976	2	47	3.5	-6.1
hp60	9.2	29.0088	40.9976	2	47	3.5	-6.1
hp61	9.0	29.0088	40.9976	2	47	3.5	-6.1
hp62	8.9	29.0089	40.9976	2	47	3.5	-6.1
hp63	8.2	29.0089	40.9976	2	47	3.6	-6.4
hp64	8.5	29.009	40.9977	2	47	3.8	-6.4
hp65	8.4	29.0092	40.9977	2	47	4.1	-6.5
hp66	7.6	29.0092	40.9977	2	47	4.1	-6.5
hp67	7.7	29.0093	40.9977	2	47	4.1	-65
hp68	7.6	29.0093	40.9977	2	47	4.1	-6.5
hp69	8.4	29.0093	40.9977	2	47	4.2	-6.5
hp70	9.8	29.0094	40.9978	2	47	4.2	-6.5
hp71	10.2	29.0094	40.9978	2	47	4.3	-6.6
hp72	9.4	29.0095	40.9978	2	47	4.3	-6.
hp73	7.9	29.0095	40.9978	2	47	4.4	-6.9
hp74	6.2	29.0096	40.9978	2	47	4.5	-6.2
hp75	4.0	29.0096	40.9978	2	47	4.5	-4.0
hp76	4.0	29.0096	40.9979	2	47	4.6	-2.5
hp77	4.0	29.0097	40.9979	2	47	4.7	-2.4
hp78	4.0	29.0097	40.9979	2	47	4.7	-2.4
hp79	4.0	29.0097	40.9979	2	47	4.7	-2.4

Table A.1. (Continued)

Name of Gauge Pt.	Depth (m)	Longitude (°)	Latitude (°)	Arrival time of initial wave (min)	Arrival time of max.wave (min)	Max. (+)ve amp. (m)	Max. (-)ve amp. (m)
hp80	4.0	29.0097	40.9979	2	47	4.7	-2.4
hp81	3.4	29.0098	40.9979	2	47	4.8	-2.4
hp82	-4.0	29.0099	40.998	47	47	4.5	0.0
hp83	5.6	29.0099	40.998	3	22	3.0	-3.4
hp84	7.3	29.01	40.9981	3	22	2.9	-3.3
hp85	8.4	29.0101	40.9981	3	22	2.9	-3.3
hp86	9.0	29.0101	40.9981	3	47	3.0	-3.2
hp87	9.8	29.0102	40.9981	3	22	2.8	-3.2
hp88	13.7	29.002	41.0078	3	21	2.8	-4.1
hp89	10.4	29.0022	41.0078	3	21	2.9	-4.3
hp90	9.1	29.0024	41.0077	3	21	2.9	-4.6
hp91	4.0	29.0026	41.0077	3	21	3.1	-2.6
hp92	-3.0	29.0029	41.0077	21	47	3.4	0.0
hp93	7.7	29.003	41.0077	3	22	3.0	-3.8
hp94	12.5	29.0036	41.0078	3	22	2.7	-3.8
hp95	4.4	29.0096	41.0074	3	22	4.3	-4.4
hp96	0.7	29.01	41.0073	4	22	4.7	-0.7
hp97	-2.7	29.0107	41.0071	0	0	0.0	0.0
hp98	-2.8	29.0112	41.0071	0	0	0.0	0.0
hp99	4.7	29.0148	40.9922	2	20	4.1	-4.7
hp100	2.3	29.0174	40.9918	2	36	4.5	-1.6
p1	2.0	29.019	40.9915	2	20	3.4	-1.4
p2	4.2	29.0204	40.9917	3	20	3.2	-2.6
p3	1.9	29.0215	40.992	3	21	3.0	-1.9
p4	2.0	29.0224	40.9929	3	36	3.5	-1.9
p5	3.0	29.0236	40.9944	3	21	4.0	-2.6
p6	1.8	29.0225	40.9952	3	21	3.7	-1.8

Table A.1. (Continued)

Name of Gauge Pt.	Depth (m)	Longitude (°)	Latitude (°)	Arrival time of initial wave (min)	Arrival time of max.wave (min)	Max. (+)ve amp. (m)	Max. (-)ve amp. (m)
p7	1.3	29.0212	40.9956	3	21	3.2	-1.3
p8	4.5	29.0197	40.9954	3	37	3.2	-2.3
p9	5.2	29.0178	40.9954	3	36	3.8	-2.6
p10	3.4	29.0176	40.9965	3	37	2.6	-3.4
p11	2.2	29.0185	40.9969	3	24	2.4	-1.4
p12	2.0	29.018	40.9974	3	24	2.4	-1.7
p13	7.2	29.0171	40.9982	3	17	1.8	-3.6
p14	6.0	29.0154	40.9999	3	39	1.8	-3.4
p15	9.8	29.0144	41.0002	3	24	1.8	-3.2
p16	12.7	29.0128	41.0002	3	23	1.7	-3.3
p17	15.4	29.0117	41.0003	3	23	1.9	-3.2
p18	18.0	29.0111	41.001	3	23	2.0	-3.0
p19	15.6	29.0104	41.0019	3	38	2.3	-3.2
p20	0.6	29.0103	41.0026	3	38	2.3	-0.6
p21	-1.1	29.0108	41.0028	16	38	3.1	0.0
p22	-1.9	29.0118	41.0027	22	38	3.2	0.0
p23	1.1	29.0129	41.0027	3	38	3.8	-1.1
p24	8.1	29.0124	41.0035	3	23	3.0	-4.1
p25	9.1	29.012	41.0042	3	38	3.0	-4.1
p26	10.6	29.0106	41.0041	3	23	2.7	-4.1
p27	4.6	29.0094	41.0044	3	38	2.6	-4.6
p28	12.2	29.0084	41.0043	3	23	2.2	-3.8
p29	5.0	29.0077	41.0052	3	22	2.5	-3.9
p30	8.2	29.0071	41.0061	3	22	2.9	-3.8
p31	5.0	29.0068	41.007	3	22	3.0	-2.3
p32	-0.9	29.0067	41.0074	15	22	3.3	0.0
p33	-2.4	29.0077	41.0073	22	22	3.7	0.0

Table A.1. (Continued)

Name of Gauge Pt.	Depth (m)	Longitude (°)	Latitude (°)	Arrival time of initial wave (min)	Arrival time of max.wave (min)	Max. (+)ve amp. (m)	Max. (-)ve amp. (m)
p34	-0.9	29.0088	41.0072	16	22	4.0	0.0
p35	8.8	29.0094	41.0078	3	22	4.1	-5.3
p36	6.6	29.0093	41.0083	3	22	4.2	-5.3
p37	6.5	29.0089	41.0086	3	22	4.0	-5.1
p38	11.6	29.0077	41.0088	3	22	3.4	-4.4
p39	9.4	29.0069	41.0096	3	22	3.0	-4.1
p40	11.7	29.0069	41.01	3	22	2.9	-3.9
p41	9.9	29.0067	41.0107	3	22	3.1	-3.9
p42	-2.7	29.0071	41.0108	21	22	3.3	0.0
p43	-2.6	29.0081	41.0094	16	22	3.8	0.0
p44	-2.5	29.0096	41.0093	16	22	3.9	0.0
p45	2.3	29.0097	41.0101	4	22	3.8	-2.3
p46	5.0	29.0088	41.0105	4	22	3.1	-2.6
p47	0.0	29.0105	41.0112	7	48	4.6	0.0
p48	11.5	29.0041	41.0096	3	22	2.6	-3.8
p49	10.8	29.0053	41.0079	3	22	3.1	-4.0
p50	12.1	29.0063	41.0058	3	22	2.7	-3.6
p51	11.7	29.0076	41.0033	3	22	2.2	-3.9
p52	11.6	29.009	41.0013	3	38	2.1	-3.3
p53	11.3	29.0104	40.9994	3	23	1.5	-3.2
p54	6.9	29.0153	40.9977	3	24	2.0	-5.1
p55	5.3	29.0164	40.9966	3	39	1.9	-3.8
p56	5.7	29.019	40.9947	2	22	2.6	-2.5
p57	6.2	29.0201	40.9931	2	20	3.0	-2.4
p58	6.0	29.0162	40.993	2	36	3.3	-5.9